
Research Articles: Cellular/Molecular

UPF1 governs synaptic plasticity through association with a STAU2 RNA granule

**Tyson E. Graber^{1,3}, Erika Freemantle², Mina Anadolu¹, Sarah Hébert-Seropian², Robyn MacAdam¹,
Unkyung Shin¹, Huy-Dung Hoang³, Tommy Alain³, Jean-Claude Lacaille² and Wayne S. Sossin¹**

¹*Department of Neurology and Neurosurgery, Montreal Neurological Institute, McGill University, Montreal, Quebec, Canada*

²*Department of Neurosciences, GRSNC, Université de Montréal, Montreal, Canada*

³*Children's Hospital of Eastern Ontario Research Institute, Department of Biochemistry, Microbiology and Immunology, University of Ottawa, Ottawa, Ontario, Canada.*

DOI: 10.1523/JNEUROSCI.0088-17.2017

Received: 11 January 2017

Revised: 13 July 2017

Accepted: 7 August 2017

Published: 18 August 2017

Author Contributions: T.E.G., E.F., J.-C.L. and W.S.S conceived the experiments and wrote the manuscript. T.E.G. performed the super-resolution, co-IP, RNA-FISH and RPM experiments. E.F. and S.H.-S performed the electrophysiology experiments. M.A., R.M. and U.S. performed AHA, Western blotting and helped with cloning and lentivirus construction. H.H. and T.A. contributed the ddPCR expertise and experiments.

Conflict of Interest: The authors declare no competing financial interests.

We would like to thank Drs. Thomas Stroh and Liliana Pedraza for helpful discussions and expert advice in regard to super-resolution imaging. We thank Mr. Congyao Zha for immunoblotting. We thank Mr. Ryan Sanford and Dr. Louis Collins for providing expertise regarding the measurement of super-resolution localization distances in 3D space and for the MATLAB script required to calculate point-to-point distances presented in Figure 3. T.E.G. was supported by Postdoctoral Fellowships from the Fonds de recherche du Québec-Santé (FRQS) and the Canadian Institutes of Health Research (CIHR). E.F. was supported by a Postdoctoral Fellowship from the FRQS. S.H.-S. was supported by Graduate Studentships from Université de Montréal and FRQS. This work was funded by CIHR and FRQS (J.-C.L. and W.S.S.). J.-C.L. is the recipient of the Canada Research Chair in Cellular and Molecular Neurophysiology and W.S.S. is a James McGill Professor.

Correspondence should be addressed to correspondence: Wayne Sossin, Montreal Neurological Institute, Room BT110, 3801 University Avenue, Montreal, Quebec, Canada, wayne.sossin@mcgill.ca

Cite as: J. Neurosci ; 10.1523/JNEUROSCI.0088-17.2017

Alerts: Sign up at www.jneurosci.org/cgi/alerts to receive customized email alerts when the fully formatted version of this article is published.

Accepted manuscripts are peer-reviewed but have not been through the copyediting, formatting, or proofreading process.

Copyright © 2017 the authors

1 **UPF1 governs synaptic plasticity through association with a STAU2 RNA granule**

2
3 **Abbreviated Title:** UPF1 regulates synaptic plasticity.

4
5 Tyson E. Graber^{1,3}, Erika Freemantle², Mina Anadolu¹, Sarah Hébert-Seropian², Robyn
6 MacAdam¹, Unkyung Shin¹, Huy-Dung Hoang³, Tommy Alain³, Jean-Claude Lacaille^{2#}
7 and Wayne S. Sossin^{1#*}

8
9 ¹Department of Neurology and Neurosurgery, Montreal Neurological Institute,
10 McGill University, Montreal, Quebec, Canada

11
12 ²Department of Neurosciences, GRSNC, Université de Montréal, Montreal,
13 Canada

14
15 ³Children's Hospital of Eastern Ontario Research Institute, Department of
16 Biochemistry, Microbiology and Immunology, University of Ottawa, Ottawa,
17 Ontario, Canada.

18
19 # equal contributors

20 *correspondence: Wayne Sossin
21 Montreal Neurological Institute
22 Room BT110
23 3801 University Avenue
24 Montreal, Quebec, Canada
25 wayne.sossin@mcgill.ca

26
27 # of pages: 47

28 # of figures: 8

29 # of words Abstract: 157
30 Introduction: 525
31 Discussion: 1407

32
33 **Conflict of Interest:** The authors declare no competing financial interests.

34
35 **Acknowledgements:**

36 We would like to thank Drs. Thomas Stroh and Liliana Pedraza for helpful discussions
37 and expert advice in regard to super-resolution imaging. We thank Mr. Congyao Zha for
38 immunoblotting. We thank Mr. Ryan Sanford and Dr. Louis Collins for providing
39 expertise regarding the measurement of super-resolution localization distances in 3D
40 space and for the MATLAB script required to calculate point-to-point distances
41 presented in Figure 3. T.E.G. was supported by Postdoctoral Fellowships from the
42 Fonds de recherche du Québec-Santé (FRQS) and the Canadian Institutes of Health
43 Research (CIHR). E.F. was supported by a Postdoctoral Fellowship from the FRQS.
44 S.H.-S. was supported by Graduate Studentships from Université de Montréal and
45 FRQS. This work was funded by CIHR and FRQS (J.-C.L. and W.S.S.). J.-C.L. is the

46 recipient of the Canada Research Chair in Cellular and Molecular Neurophysiology and
47 W.S.S. is a James McGill Professor.
48

49 **Abstract**

50 Neuronal mRNAs can be packaged in reversibly stalled polysome granules prior
51 to their transport to distant synaptic locales. Stimulation of synaptic metabotropic
52 glutamate receptors (mGluRs) reactivates translation of these particular mRNAs to
53 produce plasticity-related protein; a phenomenon exhibited during mGluR-mediated
54 long-term depression (mGluR-LTD). This form of plasticity is deregulated in Fragile X
55 Syndrome, a monogenic form of autism in humans, and understanding the stalling and
56 reactivation mechanism could reveal new approaches to therapies. Here, we
57 demonstrate that UPF1, known to stall peptide release during nonsense-mediated RNA
58 decay, is critical for assembly of stalled polysomes in rat hippocampal neurons derived
59 from embryos of either sex. Moreover, UPF1 and its interaction with the RNA binding
60 protein STAU2 are necessary for proper transport and local translation from a
61 prototypical RNA granule substrate and for mGluR-LTD in hippocampal neurons. These
62 data highlight a new, neuronal role for UPF1, distinct from its RNA decay functions, in
63 regulating transport and/or translation of mRNAs that are critical for synaptic plasticity.

64

65 **Significance Statement**

66 The elongation and/or termination steps of mRNA translation are emerging as
67 important control points in mGluR-LTD, a form of synaptic plasticity that is compromised
68 in a severe monogenic form of autism, Fragile X Syndrome. Deciphering the molecular
69 mechanisms controlling this type of plasticity may thus open new therapeutic
70 opportunities. Here, we describe a new role for the ATP-dependent helicase UPF1 and
71 its interaction with the RNA localization protein STAU2 in mediating mGluR-LTD

72 through the regulation of mRNA translation complexes stalled at the level of elongation
73 and/or termination.

74

75 **Introduction**

76 In neurons, mRNA transport and localized translation are crucial for synaptic
77 plasticity (Jung et al., 2014). Proper spatiotemporal control of translation in dendrites or
78 developing axons necessitates reliable suppression of protein synthesis during mRNA
79 transport and a mechanism for subsequent reactivation at the appropriate time and
80 destination. Most described repression mechanisms target translation initiation on
81 particular mRNAs (Jung et al., 2014) and it would follow that their transport precedes
82 polysome formation. In contrast, we and others have described a neuronal
83 ribonucleoprotein complex (a neuronal RNA granule) consisting of stalled polysomes,
84 where initiation of mRNAs has already occurred and repression is at the level of either
85 elongation or termination (Elvira et al., 2006; Darnell et al., 2011; Graber et al., 2013b).
86 The composition of the neuronal RNA granule seems to be particularly suited for the
87 fast bursts of protein synthesis that have been observed in metabotropic glutamate
88 receptor-dependent long-term depression (mGluR-LTD). This type of localized synaptic
89 plasticity requires protein synthesis yet paradoxically occurs even in the absence of
90 translation initiation, presumably due to the reactivated translation of pre-existing
91 polysomes (Graber et al., 2013b).

92 One protein implicated in stalled polysomes is the fragile X mental retardation
93 protein, FMRP (Darnell et al., 2011). A phosphorylated form of FMRP has been
94 previously linked with stalled polysomes (Ceman et al., 2003). Indeed, FMRP is

95 dephosphorylated upon mGluR stimulation and this is required for the proper synthesis
96 of proteins during mGluR-LTD (Niere et al., 2012). However, in the absence of FMRP,
97 mRNA transport is largely unaffected (Steward et al., 1998). LTD proteins in this context
98 are instead constitutively synthesized in dendrites independently of mGluR stimulation,
99 leading to enhanced LTD upon mGluR stimulation (Hou et al., 2006; Nosyreva and
100 Huber, 2006). Thus, FMRP appears to be necessary for stabilization of stalled
101 polysomes but not their initial formation. In contrast, the mRNA binding protein STAU2
102 is required for mGluR-LTD and has been associated with the transport and translation
103 of at least one FMRP and LTD target mRNA, *Map1b*, via its 3' untranslated region
104 (UTR) (Lebeau et al., 2011).

105 STAU2 interacts with the RNA decay factor UPF1 (Miki et al., 2011; Park et al.,
106 2013) and these proteins were found in the RNA granule proteome (Elvira et al., 2006;
107 El Fatimy et al., 2016). UPF1 is a critical ATPase/helicase in nonsense-mediated RNA
108 decay (NMD) pathways, where it is recruited to the stop codon through association with
109 eRF1 and is involved in recognition of improper stop codons that are often present in
110 mis-spliced mRNAs (Chang et al., 2007). One aspect of UPF1 function is to stall
111 translation through interactions with eIF3, another abundant component of RNA
112 granules (Elvira et al., 2006; Isken et al., 2008, El Fatimy et al., 2016), and to stall
113 peptide release through binding to eRF3 (Ivanov et al., 2008). These characteristics
114 made UPF1 an attractive candidate to play a mechanistic role in stalling polysomes.

115 Our results highlight a new role for UPF1 in regulating mRNA targets at the level
116 of transport and translation, distinct from its RNA decay functions and provide

117 mechanistic insights into how stalled polysomes can be formed prior to transport and re-
118 activated locally at synapses during synaptic plasticity.

119

120 **Materials & Methods**

121 Animals and cell culture

122 Sprague–Dawley rats were obtained from Charles River Canada. All animal
123 experiments were approved by the Animal Ethics Committees of the Montreal
124 Neurological Institute and Université de Montréal, and abided by the guidelines of the
125 Canadian Council on Animal Care. Rat primary hippocampal neurons were dissected
126 from embryonic day 18 Sprague–Dawley embryos of either sex and supplemented with
127 new medium (neurobasal media supplemented with 1% (v/v) N2 and
128 penicillin/streptomycin, 2% (v/v) B27 and 0.5 mM Gluta-MAX (Thermo Fisher Scientific))
129 every 6-8 d as previously described (Lebeau et al., 2011). Electrophysiology
130 experiments were performed with 18-25 days *in vitro* (DIV) dissociated hippocampal
131 neuron cultures while all other experiments were performed with 8-10 DIV cultures.
132 Neurons were plated on 12 mm poly-L-lysine-coated #1.5 German glass coverslips
133 (Neuvitro) at a density of 100,000 cells per well of a 12-well tissue culture plate. For
134 super-resolution experiments, neurons were plated on poly-L-lysine-coated LAB-TEK II
135 chambered #1.5 coverglass slides (Thermo Fisher Scientific). For knockdown
136 experiments with single RNAi transduction, cultures were transduced with an MOI of 3-
137 10. For rescue experiments with double transduction, cultures were transduced with
138 *Stau2* RNAi with an MOI of 3 and with STAU2 constructs, each with an MOI of 5 or with
139 *Upf1* RNAi with an MOI of 3 and with UPF1 rescue at an MOI of 0.5. While only a

140 subset of neurons was transduced with this MOI, they could be detected by the
141 mCHERRY expressed from a separate promoter on the lentivirus. A minimum of three
142 days was allowed for transduction and knockdown. Transduction efficiency was
143 assessed in each experiment by GFP or mCHERRY expression. HEK293T cells were
144 cultured in DMEM (Thermo Fisher Scientific) supplemented with 10% (v/v) FBS, sodium
145 pyruvate, penicillin, and streptomycin.

146

147 DNA constructs and lentiviruses

148 The GFP.STAU2.flag plasmid (expressing the human 59 kDa isoform of STAU2) has
149 been previously described (Graber et al., 2013b). C-terminally tagged UPF1.myc
150 plasmid (expressing human UPF1) was a kind gift from Dr. Luc Desgroseillers, and
151 RIP1.myc plasmid was a kind gift from Dr. Phil Barker. STAU2 C-terminal deletion and
152 domain mutation constructs were created by PCR amplification of regions using
153 GFP.STAU2.flag as template and inserting in-frame with GFP and the Flag tag. The
154 F207A ribosome binding mutation was generated by site-directed mutagenesis. Plasmid
155 sequences were verified by Sanger sequencing.

156 To efficiently knockdown STAU2 or UPF1 in rat hippocampal neurons, lentiviruses were
157 generated that express short hairpin RNA (shRNA) driven by a CMV promoter as
158 previously described (Thomas et al., 2009). A non-targeting, “scrambled” shRNA
159 sequence (AATTCTCCGAACGTGTCACGT), a sequence targeting all of the rat
160 isoforms of STAU2 (ACTAGTGGACGCTTTATAGCC), a sequence targeting rodent
161 UPF1 isoforms (AGCAGCTTGTGGTAAATATAC), or a sequence targeting rodent
162 PNRC2 (TGGTGATGGTGGTTCATAAA), designed using the Invitrogen Block-iT™

163 RNAi designer (thus minimizing the possibility of off-target designs) were cloned into a
164 lentiviral expression vector downstream of an emGFP ORF (pRRL.emGFP.shRNA). For
165 rescue experiments, the RNAi-resistant GFP.STAU2.flag or the GFP.C351.flag (UPF1
166 binding mutation) ORFs were excised by restriction digest from the pcDNA plasmids
167 used in the co-IP experiments and sub-cloned into the lentiviral expression plasmid. The
168 UPF1 rescue construct was purchased from Vectorbuilder (Santa Clara, CA) and
169 expressed mCHERRY from a viral promoter and human UPF1 from an EF1A promoter
170 (pLV[Exp]-mCherry/Neo-EF1A>hUPF1[ORF003793]*/FLAG pLV[Exp]). All clones were
171 verified by Sanger sequencing.

172 VSV G-pseudotyped virus was packaged by transient transfection of HEK293T helper
173 cells with Lipofectamine 2000 (Thermo Fisher Scientific) pMD2.g, pRSV-Rev, and
174 pMDLg/pRRE packaging plasmids together with the pRRL.emGFP.shRNA. Virus was
175 collected over 48 hours with cell debris removed by microfiltration. Virus was then
176 concentrated by centrifugation, resuspended in PBS, pH 7.3 and stored at -80 °C. Virus
177 was titered based on GFP expression in HEK293T cells. Transduction efficiency was
178 assessed in each experiment by GFP or mCHERRY expression.

179

180 Co-Immunoprecipitation and Immunoblotting

181 For experiments to determine if DHPG induced changes in phosphorylation of UPF1,
182 hippocampal cultures (10 DIV) were incubated in the presence or absence of 50 μ M (S)-
183 3,5-DHPG (Tocris Bioscience) for 10 min and then harvested, lysed in Laemmli buffer,
184 and the proteins separated by SDS-PAGE and immunoblotted first for phospho-UPF1
185 (1:500; anti-Ser1127; #0701016; Millipore) followed by anti-rabbit coupled to HRP, then

186 stripped and reblotted with anti-UPF1 (1:10,000; #ab133564, Epitomics) followed by
187 anti-rabbit coupled to HRP. To determine loading, the membrane was stripped one
188 additional time and probed with anti-GAPDH (1:1000; #sc-25778, Santa Cruz
189 Biotechnology) followed by anti-rabbit coupled to HRP.

190 For experiments to determine the effectiveness of knockdown and rescue, hippocampal
191 neurons were transduced at 7 DIV, and 3-7 days later were harvested and lysed in
192 Laemmli buffer. Antibodies described above were used along with anti-STAU2 (kind gift
193 of Dr. Michael Kiebler) and anti-PNRC2 (1:1000, #NBP1-74252, Novus Biologicals).

194 HEK293T cells were seeded in 6-well plates and transfected 24 h later with 1 µg each of
195 the appropriate plasmid. Cells were lysed in non-denaturing co-ip buffer (150 mM NaCl,
196 1 mM EDTA, 1% (v/v) Triton X-100, 50 mM Tris-HCl, pH 7.4) supplemented with Roche
197 Complete EDTA-free protease inhibitor cocktail (Roche). 200 µg of lysate was incubated
198 overnight with Flag antibody-conjugated beads (Sigma-Aldrich) followed by extensive
199 washing with lysis buffer. Immunoprecipitated Flag-tagged species were eluted from
200 beads with 2 µg/ml of Flag peptide (Sigma-Aldrich), resuspended in Laemmli buffer,
201 resolved by SDS-PAGE and transferred to PVDF membrane for Western blotting. For
202 co-IPs, membranes were probed with rabbit polyclonal anti-myc or mouse anti-Flag M2
203 monoclonal antibodies (Sigma-Aldrich) followed by anti-rabbit and anti-mouse
204 secondary antibodies conjugated to infrared dyes CF680 and CF770 (Biotium),
205 respectively. Secondary antibody detection was performed using the Licor Odyssey
206 system (LI-COR Biosciences), or standard horseradish peroxidase detection with film
207 was employed.

208

209 Ribopuromycylation and STAU2, UPF1 immunocytochemistry

210 To enrich for stalled polysomes, rat hippocampal neurons at 8–10 DIV were incubated
211 with 5 μ M homoharringtonine (HHT; Tocris Bioscience) in 1 ml of supplemented
212 neurobasal media for 10 min. Ribopuromycylation has been described before (Graber et
213 al., 2013b). Briefly, puromycin (100 μ M) and emetine (200 μ M) (both from Sigma-
214 Aldrich) were then added and the cells were incubated at 37°C for an additional 5 min.
215 Free puromycin was removed with a digitonin wash on ice and cells were fixed at room
216 temperature for 15 min with 4% paraformaldehyde/sucrose. Cells were permeabilized
217 with 0.1% Triton X-100 and blocked with 5% BSA. Puromycin was detected with 1:1,000
218 of mouse anti-puromycin for 1 hr (clone 2A4, (David et al., 2012)), UPF1 was detected
219 with 1:500 rabbit monoclonal anti-RENT1/UPF1 (Epitomics), and STAU2 was detected
220 with 1:500 rabbit anti-STAU2 (Dr. Michael Kiebler). 1:1,000 of anti-mouse or anti-rabbit
221 Alexa 568 secondary antibody was incubated with samples for 1 h (Thermo Fisher
222 Scientific). For super-resolution imaging, primary antibodies were detected by
223 incubation with 1:1,000 or 1:10,000 of anti-mouse Alexa 647 and anti-rabbit Alexa 568
224 for 1 h. To reduce antibody drift during single molecule localization, antibody-antigen
225 pairs were post-fixed for 10 min at room temperature with 4%
226 paraformaldehyde/sucrose.

227

228 AHA labelling

229 Neurons were first incubated with methionine-free HEPES-buffered solution (120 mM
230 NaCl, 5 mM KCl, 2 mM CaCl₂, 2 mM MgCl₂, 25 mM HEPES, 30 mM glucose) for 30 min
231 at 37 °C followed by addition of 5 μ M HHT and 25 μ M AHA (Thermo Fisher Scientific)

232 for 10 min. before induction with 50 μ M (S)-3,5-DHPG (Tocris Bioscience) for a further
233 10 min. DHPG was removed from the cells with one wash of PBS, and incubated for a
234 final 10 minutes with fresh AHA and HHT to resolve any DHPG-mediated increases in
235 protein synthesis. Cells were fixed as above. Subsequent detection of AHA has been
236 described previously (Graber et al., 2013b). For quantification of AHA, AHA intensity
237 was measured between 50-60 μ M from the soma boundary. All values were normalized
238 to the average intensity of the scrambled control from that experiment.

239

240 MAP1B induction

241 Neurons were incubated with HHT for 10 min before co-incubation with 50 μ M DHPG
242 for an additional 10 min. Cells were fixed as above and standard immunocytochemistry
243 was performed with 1:200 mouse anti-MAP1B clone AA6 (Santa Cruz Biotechnology)
244 and 1:1000 anti-mouse Alexa 568, both for 1 h. For quantification of MAP1B, MAP1B
245 intensity was measured between 50-60 μ M from the soma boundary. All values were
246 normalized to the average intensity of the scrambled control from that experiment.

247

248 Droplet digital RT-PCR

249 Total RNA was isolated from 2×10^6 hippocampal neurons using RNAqueous Total RNA
250 isolation kit following the manufacturer's protocol (Thermo Fisher Scientific). cDNA was
251 synthesized from 1 μ g of total RNA using Superscript II reverse transcriptase with dT₁₈
252 primer (Thermo Fisher Scientific). Standard curves and the appropriate annealing
253 temperatures were obtained by quantitative PCR (Eppendorf realplex) for the following
254 rat-specific primer sets (listed as forward, reverse) that were designed to span an intron:

255 *Map1b*: CACACGAGGGGAAGAGAAGG, TTAGTGGTTCCTGGTCCTGC; *Upf1*:
 256 GTCACAGACTCAAGATAACATCACG, GACTAAATCCTCATTACCAGAGTCA; *Stau2*:
 257 ACTCCACCTCTTCCTGTGA, CATACTCGGGTCCAGCCTTT; *Gapdh*:
 258 TCATGACCACAGTCCATGCC, ATCACGCCACAGCTTTCCAG; *Rgs4*:
 259 CATCGGCTGGGATTTCTGCT, GCTCACCTCTGGCAAGTTA; *Cplx1*:
 260 GGCATACGAGATAAGTATGGCATC, CTTCTTGGGTTCGAGTCAGGC; *Arc*:
 261 GCCAGTCTTGGGCAGCATAG, ACTGGTATGAATCACTGCTGGG; *Dexi*:
 262 AGAGGCCCGCCTGCTC, GGATCTGGCAACTCCCCATC; *Arf1*:
 263 GGCGGCCTGAGGTCTCT, TTGCCAAAAGGCCCTTGAA; *Gap43*:
 264 AGGAGGAGAAAGAAGCTGTAGAT, GTTCTTGGTCAGCCTCGGG. Droplet digital
 265 PCR was performed with varying amounts of cDNA using QX200 ddPCR EvaGreen
 266 Supermix (Bio-Rad) together with the QX200 Droplet Digital PCR system (Bio-Rad)
 267 according to the manufacturer's protocol. Following droplet generation, the PCR step
 268 was performed using a Bio-Rad C1000 thermal cycler (Bio-Rad) with the following
 269 parameters: 1 cycle at 94 °C for 1 minute, 45 cycles at 94 °C for 15 seconds followed by
 270 58 °C for 1 minute with a ramp rate of 2 °C/second, 1 cycle at 4 °C for 5 minutes, and 1
 271 cycle at 90 °C for 5 minutes. Droplets were flagged as positive or negative for PCR
 272 product using the QX200 Droplet Reader and Quantasoft software v1.7.4 was used to
 273 determine absolute copy number per microliter.

274

275 Single molecule RNA-FISH (smRNA-FISH)

276 Neurons were fixed on glass coverslips with formaldehyde as above, washed with PBS
 277 and permeabilized with 70% ethanol for at least 1 h. Neurons were re-hydrated with 10%

278 (v/v) formamide and 2X SSC (300 mM NaCl, 30 mM sodium citrate). Neurons were then
279 incubated with 25 pmols of *Map1b* Stellaris FISH probes (Biosearch Technologies) This
280 set of 48, 21-mer oligos each of which are conjugated to Quasar 570 fluorophores and
281 designed to target nucleotides 93-1726 of the 7386 nucleotide rat *Map1b* mRNA
282 (Genbank accession NM_019217). The probe sequences are as follows (5'-3'):
283 GAGGAAGGCAATTTCTGCTG,
284 ,GCAGCATGTTCAAAGTCTTC,CCAGTCTTTCTGATCTTTTG,CATGGGAGAGTCAAA
285 CTGCT,TGACTCTCTCATCTTTCACA,CTCTCTTTGGAAGTAGCTGA,GGTGTCTGAAAG
286 TCTCTTTTTT,TGGTTCAGTTTCAGTGAGTG,GATGTCTCTTCAAGCTTTGT,AGTCTG
287 AATTACACCTGCTT,AACTGCCTGTTCTAGACTTA,CTCTTCAAAAAGTCCCTGGA,CA
288 TCCCTGATTTATCTTCAT,CACTCAGCTCGTAGTAATCA,TTCATCTTGTTGGTTCTTG
289 G,CTTGTTCTTCAGGTAATC,CGGCCAAAGTTAAACCCAAG,CCAGAGGGGAAAG
290 ATCATGG,CAGGTAATCATCTCCTTCAT,GAGGATGTTTCAACTTGGGT,AGAAGCTA
291 ATCTGGACCTGG,TTGACTGTCTGGTTTTACGG,TTGTTGAACACACAGTACCC,AAA
292 GGTCAGTGGCCAAATCT,GAGGTTTGCTCATAGGTTAC,AGGTGCTGTTTCTTTAGTT
293 G,TTTTCTTGGCAGCAACATCTA,CTGTCCAAAGTCACTGACTT,CTGGGTGACATCAG
294 AAGGTA,CTACTTCCTGGAACAAGCAG,ATCAGTCGTGGTTTGTACTA,AATCGTCGT
295 AGGTTTCTGTT,ATCAATGGTGGTCTCATCTT,CTCTCTCCTCTTTAGGAATA,TTTTTC
296 CTTCTCACTTCATC,TTTTCCGCTTAACACAGGAG,ATTCCATCAGTGACTTTGTC,TC
297 TTGGGAGGGAAGAACGTT,GGAGCTGTTTCAAGAGAGAACG,GTGAAGAGTAGCTTGG
298 AGGA,CTTTGGAGGAGTGCGAATGA,GGTTGGTTAATGAGCCGAAG,GTTGATCCGA
299 TTTTGGACTT,GATGTTCTTTAGAGAGCCAC,CATGGTGAGCATTGTCAAGT,TGTCA
300 ATCTTCACGTTACCA,TCTCGGAAGTTCAGCTTTTG. To detect rat *Map2* mRNA

301 (Genbank accession NM_013066.1), a probe-set was synthesized with the following
302 Quasar 570-conjugated DNA sequences:
303 GAGGAAGGCAATTTCTGCTG,GCAGCATGTTCAAAGTCTTC,CCAGTCTTTCTGATC
304 TTTTG,CATGGGAGAGTCAAAGTCT, TGACTCTCTCATCTTTCACA,CTCTCTTTGGA
305 AGTAGCTGA,GGTGTCTGAAGTCTCTTTTTT,TGGTTCAGTTTCAGTGAGTG,GATGTC
306 TCTTCAAGCTTTGT,AGTCTGAATTACACCTGCTT,AACTGCCTGTTCTAGACTTA,CT
307 CTTCAAAAAGTCCCTGGA,CATCCCTGATTTATCTTCAT,CACTCAGCTCGTAGTAAT
308 CA,TTTTCATCTTGTTGGTTCTTGG,CTTGGTTCTTCAGGTAAGTTC,CGGCCAAAGTTAAA
309 CCCAAG,CCAGAGGGGAAAGATCATGG,CAGGTAATCATCTCCTTCAT,GAGGATGT
310 TTCAACTTGGGT,AGAAGCTAATCTGGACCTGG,TTGACTGTCTGGTTTTACGG,TTG
311 TTGAACACACAGTACCC,AAAGGTCAGTGGCCAAATCT,GAGGTTTGCTCATAGGTT
312 AC,AGGTGCTGTTTCTTTAGTTG,TTTCTTGGCAGCAACATCTA,CTGTCCAAAGTCAC
313 TGACTT,CTGGGTGACATCAGAAGGTA,CTACTTCCTGGAACAAGCAG,ATCAGTCGT
314 GGTGGTACTA,AATCGTCGTAGGTTTCTGTT,ATCAATGGTGGTCTCATCTT,CTCTC
315 TCCTCTTTAGGAATA,TTTTTCCTTCTCACTTCATC,TTTTCCGCTTAACACAGGAG,AT
316 TCCATCAGTGAAGTGGT,CTTGGGAGGGAAGAAGT,GGAGCTGTTTCAGAGAGA
317 ACG,GTGAAGAGTAGCTTGGAGGA,CTTTGGAGGAGTGCGAATGA,GGTTGGTTAAT
318 GAGCCGAAG,GTTGATCCGATTTTGGACTT,GATGTTCTTTAGAGAGCCAC,CATGGT
319 GAGCATTGTCAAGT,TGTCAATCTTCACGTTACCA,TCTCGGAAGTTCAGCTTTTG,AT
320 GCTTCCAGAAGAGGAGAC. The probes were incubated with the cells in hybridization
321 buffer (1 mg/ml yeast tRNA, 200 µg/ml BSA, 10 % [w/v] dextran sulphate, 2 mM vandl
322 ribonucleoside complex, 10% [w/v] formamide, 2X SSC) overnight in a humidified
323 chamber at 37 °C. Neurons were washed twice with 10 % (v/v) formamide, 2X SSC at

324 37 °C. Fresh GLOX buffer (0.37 mg/ml glucose oxidase, 300 AU catalase, 0.4 % (w/v)
325 glucose, 2X SSC, 10 mM Tris-HCl, pH 8.0) was added prior to mounting the coverslips
326 on glass slides for imaging.

327

328 Confocal imaging and quantitation of *Map1b* mRNA and puromycylated puncta

329 Neurons were imaged using a Zeiss LSM-710 confocal microscope with a 63X oil
330 immersion objective (NA=1.4). ImageJ was used for image post-processing (e.g.,
331 neurite straightening using the “Straighten” plugin) including quantitation. For
332 quantitation of puromycylated puncta, straightened images of neurites were thresholded
333 so that only high intensity puncta were visible, and their numbers counted and
334 normalized to neurite length. For smRNA-FISH, a Laplacian of Gaussian transformation
335 was applied to confocal images using the ImageJ plugin “LoG3D” to enhance edges of
336 individual puncta. Images were then thresholded and outline masks of puncta were
337 generated and quantitated in ImageJ using the “Analyze particles” tool.

338

339 Super-resolution imaging

340 Single-molecule localization was performed using a Vutara SR-350 STORM microscope
341 in the presence of a photo-switching buffer (20 mM MEA, 144 mM 2-mercaptoethanol, 2
342 mM cyclooctatetraene (COT), 170 AU glucose oxidase, 2000 AU catalase; all sourced
343 from Sigma-Aldrich). At least 5,000 exposure frames were taken and localizations were
344 calculated using Vutara’s proprietary algorithms. Point clouds with ball size diameter
345 reflecting localization accuracy were plotted using Vutara visualization software. A
346 stringent confidence cut-off of 0.9 was used together with post-hoc de-noising by

347 Delaunay Tessellation Field Interpolation (DTFE) to remove diffuse background
348 localizations. Localization data points (x, y, z coordinates) were exported and individual
349 RPM/UPF1 puncta were plotted with the `scatterplot3d` R package. Euclidean
350 distance between localization points in three-space were calculated using a custom
351 MATLAB script with the formula, $\sqrt{(x_2 - x_1)^2 + (y_2 - y_1)^2 + (z_2 - z_1)^2}$, and kernel
352 density estimates were plotted using the `geom_density` function of the `ggplot2` R
353 package.

354

355 Electrophysiology and mGluR-LTD

356 Coverslips with cultured hippocampal neurons were placed in a recording chamber
357 mounted on an inverted microscope equipped with epifluorescence (Nikon Eclipse Ti-
358 S). Cultures were perfused at 1 ml/min with Tyrode's solution at room temperature
359 containing (in mM) 150 NaCl, 4 KCl, 2 MgCl₂, 10 glucose, 10 HEPES, 2 CaCl₂, 0.1
360 picrotoxin, 0.001 tetrodotoxin (pH 7.37-7.41; adjusted to 295-305 mOsmol with KOH).
361 Whole-cell recordings were obtained from hippocampal neurons with borosilicate
362 micropipettes (3-7 MΩ) filled with intracellular solution containing (in mM) 125 K-
363 gluconate, 2.6 KCl, 1.3 NaCl, 10 HEPES, 4 ATP-Mg, 0.3 GTP-Na, 0.1 EGTA, 14
364 phosphocreatine-Tris, (pH 7.2-7.3; 275-280 mOsmol). Neurons were selected for
365 recordings by visual identification in phase contrast in experiments without transduction
366 and by GFP expression in transduction experiments. Recordings were made in voltage-
367 clamp mode using a Multiclamp 700B amplifier (Molecular Devices). The cell holding
368 potential was maintained at -60mV and series resistance was routinely monitored.
369 Recorded signals were low-pass filtered at 2 kHz, digitized at 20 kHz, and stored on a

370 PC using Digidata 1440A acquisition board and pClamp10 software (Molecular
371 Devices). Data were only included if the holding current (<200 pA) was stable and
372 series resistance (<32 M Ω) varied <25% of initial value.

373 Long-term depression was induced by bath application of the group I mGluR agonist
374 (S)-3,5-DHPG (100 μ M; Abcam) for 5 min. The translation inhibitors emetine (40 μ M)
375 and HHT (20 μ M) were bath-applied 10 min before, during and 30 min after DHPG
376 application. Miniature EPSCs (mEPSCs) were recorded in 5 min episodes throughout
377 the experiments. For analysis, mEPSCs were detected and measured over two 5 min
378 time periods, before (-5-0 min) and after (25-30 min) DHPG application using
379 MiniAnalysis program (Synaptosoft) after lowpass Gaussian filtering of traces at 1 kHz.
380 Detection threshold was set at 7 pA and all detected events were verified by visual
381 inspection. Cells with mEPSC frequency \leq 0.5 Hz were excluded from analysis.

382

383 Experimental Design and Statistical analysis

384 In general, all experiments were planned to have at least three replicates from separate
385 hippocampal cultures. Since for most of the experiments, the amount of error was not
386 known *a priori*, it was difficult to accomplish effective power analysis to pre-plan the
387 number of experiments. Unless otherwise stated in figure legends, statistical P-values
388 were determined using a one- (where appropriate) or two-tail, unpaired Student's t-test
389 for two group comparisons and one-way ANOVA followed by Šidák post-hoc multiple
390 comparison correction for >2 groups using Graphpad Prism v.6. For electrophysiology
391 experiments, one-tailed, paired t-tests on mEPSC parameters pre- versus post-DHPG
392 application were performed using Graphpad Prism. Any distinct analysis is described in

393 the figure legends. Bar plots are presented as the mean \pm SEM and in-text values are
394 stated as the mean \pm SD. Asterisks indicate p-values as follows: * $p < 0.05$, ** $p < 0.01$,
395 *** $p < 0.001$ and non-significant associations are denoted by “ns”. The experimenter was
396 blinded for the analysis of neurites labelled for AHA, RPM, MAP1B protein and *Map1b*
397 mRNA.

398

399 **Results**

400 UPF1 is required for the presence of stalled polysomes in neurites.

401 To examine the role of UPF1 in the generation of stalled polysomes we
402 constructed a lentivirus encoding GFP and short-hairpin RNAi targeted to *Upf1*. Three
403 days after infection of hippocampal neuron cultures, levels of UPF1 were significantly
404 decreased (50%) compared to neurons transduced with a lentivirus expressing a non-
405 targeting (scrambled) RNAi as measured by immunofluorescence (Figure 1A, B).
406 Western blotting indicated a similar decrease in UPF1 expression in total cell lysates
407 (Figure 1C). Next, we assessed the number of stalled polysomes in neurites with
408 lowered UPF1 expression using an in-situ run-off assay in hippocampal cultures. Briefly,
409 translating polysomes are allowed to complete translation in the presence of an inhibitor
410 (homoharringtonine; HHT) that prevents formation of new polysomes (Graber et al.,
411 2013b). The remaining stalled polysomes are detected by ribopuromycylation (RPM);
412 where puromycin is covalently attached to polysome-bound nascent peptide chains that
413 are fixed in position with the elongation inhibitor emetine (David et al., 2012). Reducing
414 the expression of UPF1 was sufficient to decrease the number of stalled polysomes
415 seen in distal dendrites (>50 μm from soma) by approximately 50% (Figure 1D).

416 Stimulation of mGlu receptors with DHPG can reactivate translation of stalled
417 polysomes encoding proteins required for mGluR-LTD (Graber et al., 2013b). This burst
418 of protein synthesis can be measured after first blocking initiation-dependent protein
419 synthesis with HHT, allowing ribosome run-off and then measuring new, initiation-
420 independent protein synthesis by pulsing with the methionine analogue
421 azidohomoalanine (AHA) (Graber et al., 2013b). A fluorophore is then chemically
422 attached to AHA and detected by fluorescence microscopy. Using this assay, we found
423 that decreasing expression of UPF1 blocked induction of initiation-independent
424 translation by DHPG (Figure 1E). To rule out off-target effects of our *Upf1* RNAi, we
425 rescued DHPG-induced initiation-independent protein synthesis with a lentivirus
426 expressing human UPF1, which lacks the sequence targeted by the RNAi. This vector
427 also expresses mCHERRY on a separate cistron. Expression of this lentivirus rescues
428 the knockdown of UPF1 (Figure 1F) and the activation of initiation-independent protein
429 synthesis by DHPG (Figure 1G), demonstrating that the effect of UPF1 on blocking
430 initiation-independent protein synthesis was not an off-target effect of the RNAi.

431 Knocking-down UPF1 should increase levels of mRNAs normally regulated by
432 NMD. Previously, the protein ARC, whose mRNA is a constitutive target for NMD due to
433 an intron in its 3' UTR, was shown to be upregulated when NMD is disrupted (Giorgi et
434 al, 2007). Indeed, droplet digital RT-PCR results from our UPF1 knockdowns are
435 consistent with this upregulation, with *Arc* mRNA increasing to 191 ± 8.85 percent over
436 scrambled controls, $n=2$. Could the effects we observe in UPF1 knockdowns be due to
437 upregulation of NMD targets? To assess this, we knocked-down expression of Proline-
438 rich Nuclear Receptor Coregulatory protein 2 (PNRC2), a protein that interacts with

439 UPF1 and that is required for NMD (Cho et al., 2009). While we observed an efficient
440 knockdown of PNRC2 in hippocampal neuronal cultures (Figure 2A), we saw no
441 significant change in the induction of AHA incorporation in neurites following DHPG
442 treatment in neurons lacking PNRC2 (Figure 2B). These data indicate that the observed
443 decrease in translation from reactivated stalled polysomes in UPF1 knockdowns
444 appears to be independent of its primary function in NMD.

445 One explanation for the paucity of stalled polysomes in distal dendrites lacking
446 UPF1 is that their mRNA cargo might be degraded in the soma. We therefore chose to
447 assess *Map1b* mRNA expression in this context as it encodes an essential protein for
448 the expression of mGluR-LTD and whose synthesis occurs in a rapid and highly
449 localized manner (Davidkova and Carroll, 2007; Lebeau et al., 2011; Graber et al.,
450 2013b). We have previously shown that *Map1b* mRNA is present in ribosome-
451 containing RNA granules (Lebeau et al., 2011) and undergoes initiation-independent
452 translation upon stimulation of mGlu receptors (Graber et al., 2013b) all features that
453 are consistent with stalled polysomes. Knockdown of UPF1 had no effect, however, on
454 total *Map1b* mRNA levels in neurons measured using droplet digital RT-PCR (Figure
455 2C), demonstrating that UPF1 does not directly regulate levels of *Map1b* mRNA through
456 NMD. This left the possibility that *Map1b* stalled polysomes do not form in the context of
457 decreased UPF1 expression, or form but become mis-localized. Alternatively, these
458 mRNAs may still be properly localized to the dendrite but undergo leaky, dispersed
459 translation that could explain the decrease in the number of stalled polysome puncta. To
460 test whether *Map1b* mRNA is still localized to dendrites, we looked at the sub-cellular
461 distribution of endogenous *Map1b* mRNA using single-molecule RNA fluorescence in

462 situ hybridization (smRNA-FISH) (Raj et al., 2008). In neurons expressing non-targeting
463 RNAi we were able to detect many copies of *Map1b* throughout the cell soma, with
464 some also visible in neurites (Figure 2D). Strikingly, in neurons expressing *Upf1* RNAi
465 there was a significant decrease in the number of *Map1b* messages per micron of
466 neurite length in both proximal (<50 μm) and distal (>50 μm from the soma boundary)
467 neurites, while somatic *Map1b* did not significantly change (Figure 2D).

468 Thus, we conclude that in the absence of UPF1, reactivation of stalled
469 polysomes in neuronal dendrites is inhibited, most likely due to the lack of formation
470 and/or transport of these structures into dendrites.

471 If UPF1 is critical for the stalling process, one might expect that post-translational
472 modification of UPF1 could play a role in release of the stall. Indeed, we found that
473 DHPG induced a significant dephosphorylation of UPF1 (Fig. 2E), consistent with the
474 known activation of phosphatases by DHPG (Niere et al, 2012). Thus, dephosphorylation
475 of UPF1 could play a role in the release of stalled polysomes following DHPG treatment.

476

477 UPF1 is co-localized with stalled polysomes in distal neurites.

478 UPF1 has been associated with RNA transport granules in previous studies
479 (Barbee et al., 2006; Giorgi et al., 2007) and is present in the proteomics of RNA
480 granules (Elvira et al., 2006; El Fatimy et al., 2016). We took advantage of our ability to
481 identify stalled polysomes using RPM and then assayed their association with UPF1 in
482 super-resolution using dual color, three-dimensional stochastic optical reconstruction
483 microscopy (Dual Color 3D-STORM; Figure 3) (Juetten et al., 2008). HHT-
484 ribopuromycylated neurons were fixed and probed for puromycin and UPF1 using

485 appropriate primary antibodies, incubated with standard secondary antibodies and
486 followed by an additional fixation step to minimize movement of antibody complexes.
487 Ribopuromycylated puncta in hippocampal neurons were first located by low resolution
488 wide-field immunofluorescence (Figure 3A) prior to surveying individual fluorophore-
489 conjugated secondary antibody localizations at super-resolution (Figure 3B, C). We
490 collected super-resolution localizations of both Alexa568 (labelling puromycin) and
491 Alexa647 (labelling UPF1) puncta in samples saturated with secondary antibodies (high
492 density probes at 1:1000 dilution; Figure 3B) and samples labelled with limited
493 secondary antibody (low density probes at 1:10000 dilution; Figure 3C) to minimize the
494 chances of detecting non-specific antibody complexes. Intriguingly, we found that the
495 topography of localizations, when plotted with Gaussian blur (point-splating), highlight
496 structures that are suggestive of multiple UPF1 molecules (or a single molecule
497 complexed with multiple secondary antibodies) in complex with the apex of a stalled
498 polysome (Figure 3B, C). Supporting this supposition, the sizes of the densely-
499 puromycylated structures were found to be generally uniform and consistent with the
500 expected diameter of a puromycylated ribosome with associated primary and secondary
501 antibodies (approximately 25-50 nm). We used a commercially available monoclonal
502 antibody against UPF1 whose epitope remains proprietary, therefore it is difficult to
503 determine if the granules we observed contained one or more UPF1 molecules.
504 However, we did observe, in general, fewer UPF1 relative to puromycin localizations
505 (individual localizations for a typical granule are plotted in Figure 3D). While the number
506 of puromycin localizations appears too large for a single polysome, uncertainties
507 concerning the number of secondary antibody fluorophores and the possible recounting

508 of fluorophores due to movement during the lengthy imaging procedure, preclude
509 definitive conclusions on this point. If multiple polysomes are present in a granule it
510 would suggest some tertiary organizing feature in RNA granules as has recently been
511 suggested by EM micrographs of purified RNA granules (El-Fatimy et al, 2016). Further,
512 we found that puromycin and UPF1 localizations resided in close proximity to each
513 other. We extended this qualitative analysis by calculating the point-to-point distances
514 for each localization species (UPF1-UPF1, puromycin-puromycin and UPF1-puromycin)
515 and plotting their densities as a function of distance in nanometres. Figure 3E describes
516 the distribution of the localizations found in the single puncta represented in Figure 3D.
517 By surveying the maxima of these densities for each species across multiple RPM
518 puncta from independent experiments, we observed that peak hetero-molecular (UPF1-
519 puromycin) distances were significantly different from peak homo-molecular (UPF1-
520 UPF1 or puromycin-puromycin) distances, consistent with a specific molecular complex
521 rather than non-specific association of secondary antibodies (Figure 3F). Thus, by using
522 a super-resolution approach, we were able to sufficiently resolve sub-micron,
523 anisotropic structures that are consistent with helical polysomes bound to UPF1.

524

525 Characterization of a STAU2 mutation that fails to interact with UPF1.

526 We have previously shown that STAU2, but not its paralogue STAU1, is required
527 for production of MAP1B during mGluR-LTD in rat primary hippocampal neurons and
528 slices (Lebeau et al., 2011). Consistent with this, we also found that STAU2 colocalizes
529 with ribosomes and stalled polysomes (Lebeau et al., 2011; Graber et al., 2013b). We
530 now find that similar to our results with *Upf1* RNAi, reduction of STAU2 expression

531 using RNAi targeting all major rat isoforms (Figure 4A, B), reduces the number of stalled
532 polysomes (Figure 4C) and decreases the amount of *Map1b* mRNA found in distal
533 neurites (Figure 4D). Importantly, no effect on localization was seen for *Map2* mRNA in
534 either *Stau2* or *Upf1* RNAi-expressing neurons, indicating that the mis-localization effect
535 for *Map1b* cannot be generalized to all mRNAs (Figure 4E). Similar to UPF1 (Figure
536 2C), there was no effect of knocking-down STAU2 on the total level of *Map1b* mRNA
537 despite a strong reduction (>80%) in *Stau2* mRNA (Figure 4F).

538 Together, these results suggest a functional relationship between STAU2 and
539 UPF1 in the context of RNA transport, translation, or both. Interestingly, both STAU1
540 and STAU2 have been previously implicated in RNA decay together with UPF1 where
541 their interactions were found to enhance exon-junction complex-independent RNA
542 decay (so-called Staufen-mediated RNA decay; SMD) (Park et al., 2013). This
543 interaction triggers UPF1 phosphorylation that facilitates the recruitment of RNA
544 decapping factors, although the exact mechanisms and proteins involved are still not
545 well understood (Kim et al., 2005). However, the loss of Staufen-mediated decay is
546 unlikely to explain our results as (i) in our cultures we do not observe upregulation of
547 mRNAs known to be targets of SMD after STAU2 knockdown (Figure 4F) and (ii)
548 knockdown of PNRC2 does not affect the DHPG-induced upregulation of initiation-
549 independent RNA translation (Figure 2B), even though PNRC2 is also required for SMD
550 (Cho et al., 2012). It should also be noted that neither *Upf1* mRNA, nor NMD targets
551 (*Arc*, *Dexi*) are upregulated after knockdown of STAU2, although one mRNA previously
552 shown to be regulated by STAU2, *Rgs4* (Heraud-Farlow et al, 2013), was slightly

553 downregulated, albeit non-significantly (Figure 4F). UPF1 knockdown also did not alter
554 *Stau2* mRNA levels (93.6 ± 8.7 percent of scrambled controls).

555 Using transiently expressed epitope-tagged versions of human UPF1 and the 59
556 kilodalton isoform of STAU2 (an RNA granule-associated isoform that is highly
557 expressed in hippocampal neurons (Duchaine et al., 2002)), we were able to confirm
558 their co-immunopurification in HEK293T (Figure 5A, B). Importantly, we were unable to
559 pull-down another myc-tagged protein, RIP-myc, with FLAG-tagged STAU2 indicating
560 that the STAU2-UPF1 interaction is specific (Figure 5B). Miki et al have previously
561 shown that STAU2 and UPF1 directly interact with each other in a cell-free system (Miki
562 et al, 2011). However, this interaction could depend on indirect binding through RNA or
563 RNA-ribosome complexes in HEK293T cells. To address this, we treated lysates with
564 RNase A prior to immunoprecipitation and found that despite the loss of the ribosomal
565 protein S6 (RPS6; indicative of ribosome-RNA association) in the nuclease-treated IP,
566 STAU2 complexes still contained UPF1, although we cannot say that RNA-ribosome
567 complexes do not facilitate this interaction (Figure 5C).

568 To begin to understand how STAU2-UPF1 interactions might affect mRNA
569 translation, we attempted to define the specific region(s) in the 59 kilodalton isoform of
570 human STAU2 that is necessary for binding to UPF1. We created several Flag-tagged
571 constructs that expressed STAU2 domains (incorporating the STAU2 nuclear export
572 signal to ensure cytoplasmic expression; Figure 5A). We found that on their own, none
573 of the defined double-stranded RNA binding domains (dsRBD) or the C-terminal tubulin
574 binding domain (TBD) were sufficient for interaction with UPF1 (data not shown).

575 However, a C-terminal deletion mutation that lacked the TBD (C351), but retained
576 dsRBDs 1-4 was sufficient to abrogate binding to UPF1 (Figure 5D).

577 We next asked whether the loss of UPF1 binding with the STAU2 C351 mutation
578 could be indirect, resulting from impaired STAU2 interaction with ribosome/RNA
579 complexes that are presumably pulled-down in our immunoprecipitations lacking RNase
580 A treatment. We detected the presence of ribosomal protein S6 (RPS6) in our
581 immunoprecipitated STAU2-UPF1 complexes suggesting the presence of
582 mono/polysome complexes. To confirm this, we introduced a point mutation in dsRBD3
583 of STAU2 (F207A; numbering based on Uniprot ID: Q9NUL3-2) that is analogous to the
584 F135A mutation in its paralogue STAU1 that has previously been reported to ablate
585 RNA binding and curtail binding to the ribosome, presumably by altering the secondary
586 structure of the former (Luo et al., 2002). We observed decreased affinity of this
587 mutation construct for RPS6 relative to wildtype (Figure 5D), likely due to a decrease in
588 associated mono/polysomes. Importantly however, the ability to bring down RPS6 is
589 unaffected in immunoprecipitants from cells expressing the C351 mutation vs. wildtype
590 STAU2 (Figure 5D). These data suggest that the C351 mutation does not impair STAU2
591 interactions with mono/polysomes, but does affect the interaction with UPF1, consistent
592 with an independent interaction between STAU2 and UPF1. It should be noted that the
593 C351 mutation could still affect STAU2 function(s) other than binding UPF1, such as
594 hetero-dimerization (Gleghorn et al., 2013).

595 To better define the region in the C-terminus that is necessary for UPF1 binding,
596 we created several additional C-terminal deletion mutations. Full binding,
597 indistinguishable from the wildtype, was observed in the C430 mutation which contained

598 the entire tubulin binding domain but lacked the remaining C-terminal residues (Figure
599 5E). Critically, we found that the middle portion of the tubulin binding domain (TBD) was
600 necessary, but not sufficient for efficient binding to UPF1. Interestingly, this binding
601 region has very low amino acid homology to Staufen 1 (Figure 5F) perhaps suggesting
602 that Staufen 1 and 2 interact with UPF1 in different ways, although the functional
603 significance of this, if any, remains unclear.

604

605 STAU2-UPF1 interactions are necessary for DHPG induction of MAP1B protein in distal
606 neurites

607 STAU2 is required for DHPG induction of MAP1B protein (Lebeau et al., 2011).
608 This occurs independently of translation initiation (Graber et al., 2013b) and is
609 presumably the result of peptide release from polysomes that have been reactivated. To
610 determine if the STAU2-UPF1 interaction is important for this functional release of
611 stalled polysomes, we used a rescue paradigm where STAU2 levels were reduced by
612 our lentiviral RNAi in hippocampal rat neurons and then rescued using a separate
613 lentivirus expressing either human full-length STAU2 or human STAU2 lacking the
614 UPF1 binding domain (C351) which are both resistant to rat-specific RNAi. Both
615 constructs expressed at equivalent levels (reported by GFP immunodetection in Figure
616 5G) and the full-length STAU2 construct expressed at similar levels to the endogenous
617 59 kilodalton STAU2 (top panel of Figure 5G; note the Stau2 antibody does not detect
618 C351 expression). As previously shown using transient siRNA transfection by Lebeau et
619 al, knockdown of STAU2 in this context blocked the DHPG-mediated induction of
620 MAP1B protein in distal neurites (Figure 5H). Demonstrating that this is not an off-target

621 effect, we were able to rescue induction of MAP1B with co-expression of RNAi-resistant
622 human STAU2, but not the STAU2 harbouring the C351 mutation (Figure 5H). These
623 results suggest that DHPG induction of MAP1B expression requires the STAU2-UPF1
624 interaction, although we cannot rule out the possibility that the loss of the DHPG-
625 induced increase was due to a separate function of STAU2 that was also lost with the
626 C351 mutation.

627

628 mGluR-LTD in dissociated hippocampal neurons does not require translation initiation

629 We next examined the role of UPF1 and STAU2 in regulating synaptic plasticity
630 mediated by reactivated translation from stalled polysomes. We first determined if
631 mGluR-LTD recorded at the single cell level in cultured hippocampal neurons was
632 dependent on re-activation of stalled polysomes using voltage clamp recordings of
633 miniature excitatory postsynaptic currents (mEPSCs). In cultured hippocampal neurons,
634 mGluR-LTD is associated with an internalization of GluA receptors resulting in a
635 reduction of mEPSC frequency with no change in amplitude (Waung et al., 2008;
636 Sanderson et al., 2011). Consistent with these previous reports, DHPG-induced LTD in
637 long-term hippocampal neuron cultures was associated with a decrease in mEPSC
638 frequency, but not amplitude, following bath application of DHPG (Figure 6A, B).

639 We recently showed that mGluR-LTD at Schaffer collateral synapses is
640 insensitive to HHT, an inhibitor of translation initiation or, more precisely, of the first
641 round of elongation. Furthermore, mGluR-LTD was prevented by emetine, an inhibitor
642 of translation elongation (Graber et al., 2013b). Thus, we first verified if mGluR-LTD was
643 similarly independent of translation initiation in dissociated cultured neurons. Application

644 of the elongation inhibitor emetine blocked the decrease in mEPSC frequency induced
645 by DHPG, while incubation with the initiation inhibitor HHT did not (Figure 6A, B). Mean
646 amplitude of mEPSCs was not significantly changed by DHPG in these experiments.
647 These results, showing a block of mGluR-LTD by the translation elongation inhibitor
648 emetine confirm that long-term synaptic plasticity in cultured hippocampal neurons is
649 dependent on *de novo* protein synthesis. Moreover, the lack of inhibition of mGluR-LTD
650 by the translation initiation inhibitor HHT, suggests that this plasticity is dependent on
651 regulation downstream of initiation, through reactivated translation from stalled
652 polysomes.

653

654 UPF1 and its interaction with STAU2 are required for mGluR-LTD in hippocampal
655 neurons

656 Having established that cultured neurons show mGluR-LTD independent of
657 translation initiation, but dependent on translation elongation in response to DHPG, we
658 next wanted to determine if UPF1, and its interaction with STAU2 on stalled polysomes,
659 were required for mGluR-LTD. We assessed DHPG-induced LTD of mEPSCs in
660 neurons expressing *Upf1* or scrambled RNAi lentivirus and found that the depression of
661 mEPSC frequency, without change in amplitude, was prevented in neurons with
662 reduced UPF1 expression relative to those expressing scrambled RNAi (Figure 7A, B).

663 We previously reported that mGluR-LTD induced by DHPG was impaired in cultured
664 hippocampal slices transiently transfected with *Stau2* siRNA (Lebeau et al., 2011). Next,
665 we verified the importance of STAU2 in mGluR-LTD in dissociated neurons using *Stau2*
666 RNAi lentivirus. Neurons expressing *Stau2* RNAi did not show DHPG-induced

667 depression of mEPSC frequency, consistent with our previous observations in slices
668 (Figure 7A, B). There was, however an increase in EPSP amplitudes when *Stau2* was
669 knocked-down, that was not seen with UPF1. This may be due to regulation of
670 additional messages by STAU2 independent of its role in stalled polysomes (Heraud-
671 Farlow et al., 2013). Indeed, our droplet digital RT-PCR results revealed that one of the
672 previously identified STAU2 mRNA targets was slightly downregulated in STAU2
673 knockdowns (*Rgs4*; Fig 4F). Decreases in this and presumably other proteins stabilized
674 by STAU2 may underlie the changes in amplitude seen with its loss, but not with that of
675 UPF1.

676 Next, we attempted to rescue the deficit in mGluR-LTD in neurons expressing
677 *Stau2* RNAi with lentiviruses that express RNAi-resistant human STAU2. Infection with
678 STAU2-expressing virus restored the DHPG-induced LTD of mEPSC frequency
679 indicating that the *Stau2* RNAi phenotype was not due to off-target effects (Figure 7A,
680 B). Finally, we sought to determine whether the UPF1-STAU2 interaction was
681 necessary for the STAU2 rescue of mGluR-LTD by expressing the STAU2 C351
682 mutation which cannot interact with UPF1 into the *Stau2* RNAi background. Expression
683 of the mutated STAU2 failed to rescue the DHPG-induced LTD of mEPSC frequency
684 (Figure 7A, B). Interestingly, the mutated STAU2 did rescue the change in mEPSC
685 amplitude, consistent with this effect of STAU2 being mediated through a UPF1-
686 independent role of STAU2 and also demonstrating that the C351 mutation does not
687 perturb all STAU2 functions.

688 Together, these data demonstrate that UPF1, as well as STAU2, are required for
689 mGluR-LTD in hippocampal neurons and moreover, highlight the importance of their

690 direct interaction in the transport and/or translation of RNA granules that participate in
691 protein synthesis-dependent synaptic plasticity.

692

693 **Discussion**

694 A new role for UPF1 in the formation of neuronal granules comprising stalled polysomes

695 We've characterized a novel function for the RNA helicase UPF1 in the
696 regulation of transport RNA granules consisting of stalled polysomes in neurons. UPF1
697 is present in stalled polysomes by proteomic analysis (Elvira et al., 2006; El Fatimy et
698 al., 2016) and we demonstrate it occupies a polarized position in neuronal RNA
699 granules determined using super-resolution microscopy (Figure 3). Knockdown of UPF1
700 in hippocampal neurons results in: i) fewer stalled polysomes in neurites, ii) reduced
701 transport of *Map1b*, an mRNA stored in stalled polysomes, iii) ablation of DHPG-
702 induced, initiation-independent protein synthesis (Figure 1), and iv) a block in mGluR-
703 LTD expression, which is known to involve stalled polysomes (Figure 7). Together,
704 these data strongly argue for the importance of UPF1 in this form of regulated transport
705 and translation in neurons.

706 There are a number of possible functions for UPF1 in regulating stalled
707 polysomes: UPF1 may be important in their formation, stability, ability to be
708 translationally activated, or some combination thereof. One attractive model would be
709 that when a ribosome translating an mRNA reaches the stop codon, UPF1 is recruited
710 together with the peptide release factors eRF1 and eRF3, and instead of signalling
711 decay or stimulating release as in non-neuronal cells, a process initiating the formation
712 of a stalled polysome would ensue. Such a mechanism would also require STAU2,

713 mediating either UPF1 recruitment or stabilization and may require additional, neuron-
714 specific trans-acting proteins or regulatory RNAs, or cis-acting sequence factors such
715 as alternative 3' UTRs.

716 It is possible that the effect of knocking-down UPF1 indirectly regulates stalled
717 polysomes; mRNAs normally targeted for NMD through the presence of introns in their
718 3' UTRs may be longer-lived, thus exhibiting enhanced translation in this context
719 (Kurosaki and Maquat, 2013). However, the best-known LTD-related protein that is also
720 a NMD target, ARC (Giorgi et al., 2007), would have been expected to facilitate mGluR-
721 LTD by its increased levels in neurons lacking sufficient UPF1, not lead to a loss of
722 mGluR-LTD like we observed. Moreover, decreases in *Map1b* mRNA localization to
723 dendrites would be difficult to explain by a loss of NMD-mediated *Map1b* degradation.
724 Finally, in our effort to dissect disparate UPF1 functions, knockdown of PNRC2, a
725 protein that mediates decapping as part of the NMD/SMD function of UPF1 had no
726 effect on translation from reactivated stalled polysomes (new Figure 2). These data
727 strongly support the concept that the canonical NMD/SMD functions of UPF1 do not
728 play a role in DHPG-mediated changes in translation of plasticity-related proteins. It
729 remains to be seen whether these roles can be dissected in the context of synaptic
730 plasticity and in particular mGluR-LTD.

731 Perhaps the most parsimonious conclusion drawn from the observed reduction in
732 *Map1b* mRNA copy number and translation in neurites with reduced UPF1 expression,
733 is that the latter functions in *Map1b* RNA transport rather than translation *per se*. This
734 could occur in a number of ways. First, UPF1 interactions might be a pre-requisite for
735 proper transport of a *Map1b* stalled polysome. Second, UPF1 interactions might be

736 required for stalled polysome formation, without which *Map1b* becomes mis-localized.
737 CLIP analysis has shown that UPF1 interacts with mRNA in both EJC-dependent and
738 independent manners such that many copies of UPF1 proteins are scattered throughout
739 the message (Hurt et al., 2013; Zund et al., 2013). Importantly, Zund et al showed that
740 UPF1 is preferentially displaced from coding regions on mRNAs with associated
741 ribosomes while binding in 3' UTRs is retained. This observation is consistent with our
742 super-resolution data showing a large number of UPF1 localizations at the apical end of
743 a polysomal structure. UPF1 does indeed specifically interact with the *Map1b* 3' UTR
744 (Hurt et al., 2013) so it is certainly possible that downregulation of the former could
745 affect the transport of *Map1b* stalled polysomes, possibly by disturbing Staufen binding
746 sites. Importantly however, UPF1 (or STAU2) knockdown does not appear to adversely
747 affect steady-state levels of *Map1b* in neurons (Figure 2C, 4F). These data suggest that
748 the NMD functions of UPF1, whether direct or indirect are not involved in this context
749 and highlight a tantalizing new function for this protein.

750

751 Implications of a role for STAU2-UPF1 interactions in RNA granules

752 The interaction between STAU2 and UPF1 has now been seen in a number of
753 independent studies (Miki et al., 2011; Park et al., 2013; Flury et al., 2014). A previous
754 study, however, identified the dsRBD2 and dsRBD3 domains as sufficient to bind to
755 UPF1 and did not require C-terminal domains (Miki et al., 2011). In contrast, we found
756 that deletion of the C-terminus up to and including the TBD almost completely removed
757 UPF1 binding without affecting STAU2 interactions with the ribosome. These results are
758 not necessarily contradictory and suggest the possibility of two interacting domains, one

759 including dsRBD2 and dsRBD3 and the second involving the TBD, both of which are
760 required for full binding. For the purposes of our study, the loss of interaction with the
761 removal of the C-terminal (C351 mutation) allowed us to more specifically examine the
762 role of STAU2-UPF1 interactions, since disrupting dsRBD3 would confound
763 interpretation by removing most dsRNA binding for STAU2, including association with
764 the ribosome (Luo et al., 2002). The TBD and dsRBD4 were sufficient for binding of
765 STAU1 to UPF1 (Kim et al., 2005), although we show that removing the TBD was
766 sufficient to prevent binding even in the presence of dsRBD4. Previous reports indicate
767 that STAU2 binds to UPF1 more effectively than STAU1 (Park et al., 2013; Flury et al.,
768 2014), and this may be explained either by the additional binding site in dsRBD2 or
769 dsRBD3, or differences in the TBD involved in UPF1 binding (see Figure 5F for a
770 clustalW alignment of STAU2 vs. STAU1 that shows the low percent identity of residues
771 in this region).

772

773 Implications for the release of stalled polysomes

774 mGluR-LTD requires fast, local translation (Huber et al., 2000). We have
775 previously shown that this translation is independent of translation initiation (Graber et
776 al., 2013b), suggesting that LTD proteins are generated by finishing translation of
777 previously initiated mRNAs. Based on our data and previous studies, we propose that at
778 least three interlocked mechanisms could be implicated in releasing this form of stalled
779 translation. Phosphorylated FMRP is necessary for stalling or stabilization of stalled
780 polysomes and FMRP dephosphorylation is required for mGluR-LTD, presumably by
781 releasing the FMRP-mediated “brake” on stalled polysomes (Richter and Collier, 2015).

782 Second, eEF2 phosphorylation is required for mGluR-LTD and although the underlying
783 reasons are still unclear, it is possible that this is due to a requirement for release of
784 stalled polysomes (Graber et al., 2013a). Indeed, other forms of plasticity that require
785 eEF2 phosphorylation also appear to be due to a need for reactivation of stalled
786 polysomes (McCamphill et al., 2015). If release of mRNAs is stalled through UPF1-
787 STAU2 interactions, then this would also be subject to signal transduction mechanisms
788 induced by mGluR-LTD. Interestingly, we also observe dephosphorylation of UPF1 after
789 induction of mGluR-LTD (Figure 2). Alternatively, once initially stalled through UPF1-
790 STAU2 interactions, FMRP- and eEF2-mediated controls may predominate in the
791 transported RNA granule. The role of UPF1-STAU2 interactions in release of a stalled
792 polysome will be difficult to dissect if, as we suggest in this study, the latter do not form
793 in the absence of this interaction.

794

795 A new role for UPF1 in long-term synaptic plasticity

796 It has been suggested that specific transport complexes are involved in distinct
797 forms of plasticity. We have previously shown that STAU2 is required for mGluR-LTD
798 (Lebeau et al., 2011), while the paralogous STAU1 is necessary for the late phase of
799 NMDA receptor-dependent long-term potentiation (late-LTP) (Lebeau et al., 2008).
800 Interestingly, while late-LTP and mGluR-LTD both require protein synthesis, late-LTP is
801 blocked by *either* translation initiation *or* elongation inhibitors in contrast to mGluR-LTD,
802 which is blocked only by elongation inhibitors (Graber et al., 2013b). Since both STAU1
803 and STAU2 can bind to UPF1 (Park et al., 2013; Flury et al., 2014), our finding that
804 mGluR-LTD requires the UPF1-STAU2 interaction raises the intriguing possibility that

805 UPF1-STAU1 complexes might function in late-LTP. However, it remains to be
806 determined how such a differential interaction by UPF1 may regulate the translation of
807 different subsets of mRNAs in mGluR-LTD and late-LTP. Thus, it would be of interest to
808 explore how a differential interaction of UPF1 with either STAU1 or STAU2 may
809 regulate the synthesis of distinct plasticity related proteins through stalled polysomes,
810 and direct the switch between long-term synaptic depression and potentiation.

811

812 **Author Contributions**

813 T.E.G., E.F., J.-C.L. and W.S.S conceived the experiments and wrote the manuscript.
814 T.E.G. performed the super-resolution, co-IP, RNA-FISH and RPM experiments. E.F.
815 and S.H.-S performed the electrophysiology experiments. M.A., R.M. and U.S.
816 performed AHA, Western blotting and helped with cloning and lentivirus construction.
817 H.H. and T.A. contributed the ddPCR expertise and experiments.

818

819 **References**

820

821 Barbee SA, Estes PS, Cziko AM, Hillebrand J, Luedeman RA, Coller JM, Johnson N,
822 Howlett IC, Geng C, Ueda R, Brand AH, Newbury SF, Wilhelm JE, Levine RB,
823 Nakamura A, Parker R, Ramaswami M (2006) Staufen- and FMRP-containing
824 neuronal RNPs are structurally and functionally related to somatic P bodies.
825 Neuron 52:997-1009.

826 Ceman S, O'Donnell WT, Reed M, Patton S, Pohl J, Warren ST (2003) Phosphorylation
827 influences the translation state of FMRP-associated polyribosomes. Hum Mol
828 Genet 12:3295-3305.

- 829 Chang YF, Imam JS, Wilkinson MF (2007) The nonsense-mediated decay RNA
830 surveillance pathway. *Annu Rev Biochem* 76:51-74.
- 831 Cho H, Kim KM, Kim YK (2009) Human proline-rich nuclear receptor coregulatory
832 protein 2 mediates an interaction between mRNA surveillance machinery and
833 decapping complex. *Mol Cell* 33:75-86.
- 834 Cho H, Kim KM, Han S, Choe J, Park SG, Choi SS, Kim YK (2012) Staufen1-mediated
835 mRNA decay functions in adipogenesis. *Mol Cell* 46:495-506.
- 836 Darnell JC, Van Driesche SJ, Zhang C, Hung KY, Mele A, Fraser CE, Stone EF, Chen
837 C, Fak JJ, Chi SW, Licatalosi DD, Richter JD, Darnell RB (2011) FMRP stalls
838 ribosomal translocation on mRNAs linked to synaptic function and autism. *Cell*
839 146:247-261.
- 840 David A, Dolan BP, Hickman HD, Knowlton JJ, Clavarino G, Pierre P, Bennink JR,
841 Yewdell JW (2012) Nuclear translation visualized by ribosome-bound nascent
842 chain puromycylation. *J Cell Biol* 197:45-57.
- 843 Davidkova G, Carroll RC (2007) Characterization of the role of microtubule-associated
844 protein 1B in metabotropic glutamate receptor-mediated endocytosis of AMPA
845 receptors in hippocampus. *J Neurosci* 27:13273-13278.
- 846 Duchaine TF, Hemraj I, Furic L, Deitinghoff A, Kiebler MA, DesGroseillers L (2002)
847 Staufen2 isoforms localize to the somatodendritic domain of neurons and interact
848 with different organelles. *J Cell Sci* 115:3285-3295.
- 849 El Fatimy R, Davidovic L, Tremblay S, Jaglin X, Dury A, Robert C, De Koninck P,
850 Khandjian EW (2016) Tracking the Fragile X Mental Retardation Protein in a

- 851 Highly Ordered Neuronal RiboNucleoParticles Population: A Link between
852 Stalled Polyribosomes and RNA Granules. *PLoS Genet* 12:e1006192.
- 853 Elvira G, Wasiak S, Blandford V, Tong XK, Serrano A, Fan X, del Rayo Sanchez-
854 Carbente M, Servant F, Bell AW, Boismenu D, Lacaille JC, McPherson PS,
855 DesGroseillers L, Sossin WS (2006) Characterization of an RNA granule from
856 developing brain. *Mol Cell Proteomics* 5:635-651.
- 857 Flury V, Restuccia U, Bachi A, Muhlemann O (2014) Characterization of
858 phosphorylation- and RNA-dependent UPF1 interactors by quantitative
859 proteomics. *J Proteome Res* 13:3038-3053.
- 860 Giorgi C, Yeo GW, Stone ME, Katz DB, Burge C, Turrigiano G, Moore MJ (2007) The
861 EJC factor eIF4AIII modulates synaptic strength and neuronal protein
862 expression. *Cell* 130:179-191.
- 863 Gleghorn ML, Gong C, Kielkopf CL, Maquat LE (2013) Staufen1 dimerizes through a
864 conserved motif and a degenerate dsRNA-binding domain to promote mRNA
865 decay. *Nat Struct Mol Biol* 20:515-524.
- 866 Graber TE, McCamphill PK, Sossin WS (2013a) A recollection of mTOR signaling in
867 learning and memory. *Learn Mem* 20:518-530.
- 868 Graber TE, Hebert-Seropian S, Khoutorsky A, David A, Yewdell JW, Lacaille JC, Sossin
869 WS (2013b) Reactivation of stalled polyribosomes in synaptic plasticity. *Proc Natl*
870 *Acad Sci U S A* 110:16205-16210.
- 871 Heraud-Farlow JE, Sharangdhar T, Li X, Pfeifer P, Tauber S, Orozco D, Hormann A,
872 Thomas S, Bakosova A, Farlow AR, Edbauer D, Lipshitz HD, Morris QD, Bilban

- 873 M, Doyle M, Kiebler MA (2013) Staufen2 regulates neuronal target RNAs. *Cell*
874 *Rep* 5:1511-1518.
- 875 Hou L, Antion MD, Hu D, Spencer CM, Paylor R, Klann E (2006) Dynamic translational
876 and proteasomal regulation of fragile X mental retardation protein controls
877 mGluR-dependent long-term depression. *Neuron* 51:441-454.
- 878 Huber KM, Kayser MS, Bear MF (2000) Role for rapid dendritic protein synthesis in
879 hippocampal mGluR-dependent long-term depression. *Science* 288:1254-1257.
- 880 Hurt JA, Robertson AD, Burge CB (2013) Global analyses of UPF1 binding and function
881 reveal expanded scope of nonsense-mediated mRNA decay. *Genome Res*
882 23:1636-1650.
- 883 Isken O, Kim YK, Hosoda N, Mayeur GL, Hershey JW, Maquat LE (2008) Upf1
884 phosphorylation triggers translational repression during nonsense-mediated
885 mRNA decay. *Cell* 133:314-327.
- 886 Ivanov PV, Gehring NH, Kunz JB, Hentze MW, Kulozik AE (2008) Interactions between
887 UPF1, eRFs, PABP and the exon junction complex suggest an integrated model
888 for mammalian NMD pathways. *EMBO J* 27:736-747.
- 889 Juette MF, Gould TJ, Lessard MD, Mlodzianoski MJ, Nagpure BS, Bennett BT, Hess
890 ST, Bewersdorf J (2008) Three-dimensional sub-100 nm resolution fluorescence
891 microscopy of thick samples. *Nat Methods* 5:527-529.
- 892 Jung H, Gkogkas CG, Sonenberg N, Holt CE (2014) Remote control of gene function by
893 local translation. *Cell* 157:26-40.
- 894 Kim YK, Furic L, Desgroseillers L, Maquat LE (2005) Mammalian Staufen1 recruits Upf1
895 to specific mRNA 3'UTRs so as to elicit mRNA decay. *Cell* 120:195-208.

- 896 Kurosaki T, Maquat LE (2013) Rules that govern UPF1 binding to mRNA 3' UTRs. Proc
897 Natl Acad Sci U S A 110:3357-3362.
- 898 Lebeau G, Maher-Laporte M, Topolnik L, Laurent CE, Sossin W, Desgroseillers L,
899 Lacaille JC (2008) Staufen1 regulation of protein synthesis-dependent long-term
900 potentiation and synaptic function in hippocampal pyramidal cells. Mol Cell Biol
901 28:2896-2907.
- 902 Lebeau G, Miller LC, Tartas M, McAdam R, Laplante I, Badeaux F, DesGroseillers L,
903 Sossin WS, Lacaille JC (2011) Staufen 2 regulates mGluR long-term depression
904 and Map1b mRNA distribution in hippocampal neurons. Learn Mem 18:314-326.
- 905 Luo M, Duchaine TF, DesGroseillers L (2002) Molecular mapping of the determinants
906 involved in human Staufen-ribosome association. Biochem J 365:817-824.
- 907 McCamphill PK, Farah CA, Anadolu MN, Hoque S, Sossin WS (2015) Bidirectional
908 regulation of eEF2 phosphorylation controls synaptic plasticity by decoding
909 neuronal activity patterns. J Neurosci 35:4403-4417.
- 910 Miki T, Kamikawa Y, Kurono S, Kaneko Y, Katahira J, Yoneda Y (2011) Cell type-
911 dependent gene regulation by Staufen2 in conjunction with Upf1. BMC Mol Biol
912 12:48.
- 913 Niere F, Wilkerson JR, Huber KM (2012) Evidence for a fragile X mental retardation
914 protein-mediated translational switch in metabotropic glutamate receptor-
915 triggered Arc translation and long-term depression. J Neurosci 32:5924-5936.
- 916 Nosyreva ED, Huber KM (2006) Metabotropic receptor-dependent long-term depression
917 persists in the absence of protein synthesis in the mouse model of fragile X
918 syndrome. J Neurophysiol 95:3291-3295.

- 919 Park E, Gleghorn ML, Maquat LE (2013) Staufen2 functions in Staufen1-mediated
920 mRNA decay by binding to itself and its paralog and promoting UPF1 helicase
921 but not ATPase activity. *Proc Natl Acad Sci U S A* 110:405-412.
- 922 Raj A, van den Bogaard P, Rifkin SA, van Oudenaarden A, Tyagi S (2008) Imaging
923 individual mRNA molecules using multiple singly labeled probes. *Nat Methods*
924 5:877-879.
- 925 Richter JD, Collier J (2015) Pausing on Polyribosomes: Make Way for Elongation in
926 Translational Control. *Cell* 163:292-300.
- 927 Sanderson TM, Collingridge GL, Fitzjohn SM (2011) Differential trafficking of AMPA
928 receptors following activation of NMDA receptors and mGluRs. *Mol Brain* 4:30.
- 929 Steward O, Bakker CE, Willems PJ, Oostra BA (1998) No evidence for disruption of
930 normal patterns of mRNA localization in dendrites or dendritic transport of
931 recently synthesized mRNA in FMR1 knockout mice, a model for human fragile-X
932 mental retardation syndrome. *Neuroreport* 9:477-481.
- 933 Thomas S, Ritter B, Verbich D, Sanson C, Bourbonniere L, McKinney RA, McPherson
934 PS (2009) Intersectin regulates dendritic spine development and somatodendritic
935 endocytosis but not synaptic vesicle recycling in hippocampal neurons. *J Biol*
936 *Chem* 284:12410-12419.
- 937 Waung MW, Pfeiffer BE, Nosyreva ED, Ronesi JA, Huber KM (2008) Rapid translation
938 of Arc/Arg3.1 selectively mediates mGluR-dependent LTD through persistent
939 increases in AMPAR endocytosis rate. *Neuron* 59:84-97.

940 Zund D, Gruber AR, Zavolan M, Muhlemann O (2013) Translation-dependent
941 displacement of UPF1 from coding sequences causes its enrichment in 3' UTRs.
942 Nature structural & molecular biology 20:936-943.
943

944

945 **Legends**

946

947 **Figure 1. UPF1 is required for DHPG-mediated reactivation of translation from**
948 **stalled polysomes in neurites. (A)** Schema of the lentivirus transduction protocol to
949 efficiently express shRNA targeting *Upf1* or a non-targeting control (scrambled RNAi) in
950 primary neurons. Lentivirus expression was monitored with an emGFP ORF fused
951 upstream of the shRNA cassette. Neurons were cultured for an additional 72 h prior to
952 fixation. **(B)** Representative confocal images (left) and quantitation (right) of UPF1
953 protein in neurons at Day 10 expressing indicated RNAi. Data is from 12 individual
954 neurons from three independent experiments. See Materials and Methods for
955 explanatory notes regarding statistics used throughout the article. **(C)** Immunoblot (IB)
956 showing steady-state levels of UPF1 in neurons expressing RNAi. GAPDH was used as
957 a loading control. Apparent molecular weight is indicated on left in kilodaltons (kDa).
958 Data is representative of three independent experiments. **(D)** Reduced UPF1
959 expression decreases the number of stalled polysomes in neurites. Representative
960 confocal images of straightened neurites (left) and quantitation (right) of stalled
961 polysomes more than 50 μm from the cell soma detected by ribopuromycylation in the
962 presence of HHT (see text for details). Data are from 15-24 neurons from three different
963 cultures. **(E)** UPF1 is required for mGluR-mediated, initiation-independent protein
964 synthesis. AHA incorporation (Click-AHA) into nascent peptides was measured in distal
965 neurites in the presence of HHT following activation of mGluR with 50 μM DHPG in
966 neurons expressing indicated RNAi. Data are from 30-49 neurons from four different

967 cultures. See methods for quantification. (F) Rescue of UPF1 levels in hippocampal
968 cultures. Neurons were transduced with scrambled, *Upf1* RNAi, or *Upf1* RNAi plus a
969 lentivirus expressing mCHERRY and human UPF1 ORFs (resistant to rat *Upf1* RNAi)
970 from separate promoters. Neurons from three independent cultures were fixed and
971 stained with anti-UPF1 and imaged for emerald GFP (emGFP; reporting RNAi cassette)
972 and mCHERRY (reporting UPF1 rescue cassette). Average levels of UPF1 from 10 cell
973 bodies transduced with *Upf1* RNAi or *Upf1* RNAi + UPF1 rescue lentiviruses were
974 standardized to average UPF1 levels in 10 scrambled RNAi-transduced neurons from
975 cultures transduced at the same time. Results are from three independent neuron
976 cultures. (G) Same as (E) but with expression of both *Upf1* RNAi plus UPF1 rescue
977 plasmid. Expression of UPF1 rescued the ability of DHPG to induce increased
978 incorporation of AHA. Data are from 15-26 neurons from three different cultures.

979

980 **Figure 2. DHPG-mediated translation occurs independently of NMD and requires**
981 **UPF1 for proper localization of a target mRNA.**

982 (A) Cartoon depicting function of PNRC2, acting as a bridge between the decapping
983 and NMD (or SMD) machineries on a mRNA substrate (top). Representative
984 immunoblot of PNRC2 in neurons expressing indicated RNAi (bottom). (B) PNRC2-
985 dependent NMD is not required for mGluR-mediated, initiation-independent protein
986 synthesis. The AHA incorporation assay was performed as in Figure 1E on neurons
987 expressing scrambled or *Pnrc2* RNAi. Data are from 19-29 neurons from three
988 independent cultures. (C) Droplet digital RT-PCR of *Map1b* (left) or *Upf1* (right) mRNAs
989 normalized to *Gapdh* mRNA from total lysates of hippocampal neurons expressing

990 RNAi. Data are from three independent experiments. A one-tailed t-test was used to
991 determine significance of *Upf1* knockdown. **(D)** Reduced UPF1 expression decreases
992 the number of *Map1b* mRNA copies in neurites determined using single molecule RNA-
993 FISH. Representative confocal images of straightened neurites after application of a
994 Laplacian of Gaussian transformation to highlight mRNA puncta edges are shown.
995 Segmentation and thresholding of individual puncta (“particle mask”) allowed
996 quantitation of mRNA in the soma, proximal, and distal neurites (lower panels). Data are
997 from 20-39 neurons obtained from three different cultures. **(E)** Immunoblot of total
998 neuronal lysates showing effect of DHPG on total and phospho-UPF1 (P-UPF1) levels
999 (top) and quantitation from 4 independent experiments showing change in
1000 phospho:total-UPF1 and UPF1:GAPDH expression following 50 μ M DHPG treatment for
1001 10 minutes (bottom). A one-sample, two-tailed t-test was used to determine
1002 significance.

1003

1004 **Figure 3. Super-resolution microscopy reveals stalled polysomes colocalized with**
1005 **UPF1 in distal neurites.** **(A)** Stalled polysome puncta were first detected in widefield
1006 fluorescence mode on the Vutara Stochastic Optical Reconstruction Microscope
1007 (STORM) using ribopuromycylation (RPM) in the presence of HHT (the location of an
1008 RPM puncta is indicated by arrowheads in each channel) prior to acquisition of the
1009 super-resolution image in both channels. Note that UPF1 signal was below detection
1010 during widefield acquisition due to the short exposure times needed to minimize
1011 bleaching. **(B)** Reconstructed image of a RPM puncta based on two-color localizations
1012 in three dimensions (Dual Color 3D STORM) using high density secondary antibodies to

1013 detect anti-puromycin and anti-UPF1 primary antibodies. Individual fluorophore
1014 localizations on conjugated secondary antibodies plotted using the point-splating
1015 feature of the Vutara software in order to highlight structure. Top, side, and angled
1016 views shown. (C) As in (B) but using 1:10,000 instead of 1:1,000 secondary antibody
1017 dilution. (D) Individual fluorophore localizations of the polysome-UPF1 complex in (C).
1018 (E) Kernel density plot summarizing point-to-point distances of localizations shown in
1019 (D). Vertical lines indicate density maxima at distance x (“peak density distance”). (F)
1020 Peak density distances for a population of polysome-UPF1 complexes ($n=13$) with the
1021 mean indicated by a horizontal bar. A Kruskal-Wallis non-parametric ANOVA was
1022 performed with Dunn’s multiple comparisons post-hoc test. Data were collected from
1023 three different neuronal cultures.

1024

1025 **Figure 4. STAU2 is required for the presence of stalled polysomes in neurites.** (A)
1026 STAU2 protein was knocked-down with the same lentivirus RNAi strategy as outlined in
1027 Figure 1A. Representative confocal images (left) and quantitation (right) of STAU2
1028 protein in neurons expressing indicated RNAi. (B) Representative Immunoblot showing
1029 steady-state levels of STAU2 isoforms in neurons expressing RNAi. GAPDH was used
1030 as a loading control. (C) Reduced STAU2 expression decreases the number of stalled
1031 polysomes in neurites. Representative confocal images of straightened neurites (left)
1032 and quantitation (right) of stalled polysomes more than 50 μm from the cell soma
1033 detected by ribopuromycylation (see text for details) in the presence of HHT. Data were
1034 obtained from 15-24 neurons from three different cultures. (D) Reduced STAU2
1035 expression decreases the number of *Map1b* mRNA copies in neurites determined using

1036 single molecule RNA-FISH. Representative confocal images of straightened neurites
1037 after application of a Laplacian of Gaussian transformation to highlight mRNA puncta
1038 edges are shown. Segmentation and thresholding of individual puncta (“particle mask”)
1039 allowed quantitation of mRNA in the soma, proximal, and distal neurites (lower panels).
1040 Data were obtained from 20-39 neurons from three different cultures. (E) Quantitation of
1041 *Map2* single molecule RNA-FISH puncta in neurons expressing indicated RNAi and
1042 analyzed as in (D). Data are from 3-4 neurons from 2 different cultures. (F) Expression
1043 of target mRNAs in total hippocampal neuron lysates expressing *Stau2* vs. scrambled
1044 RNAi measured by droplet digital RT-PCR. Expression of each indicated PCR target
1045 was normalized to *Gapdh*. A one-sample, two-tailed t-test was used to determine
1046 significance, n=3-4 independent cultures.

1047

1048 **Figure 5. UPF1 interacts with the tubulin binding domain of STAU2.** (A) Schematic
1049 of DNA constructs used for co-immunoprecipitation (co-IP) assays. NES, Nuclear
1050 Export Signal; dsRBD, double-stranded RNA binding domain; TBD, tubulin binding
1051 domain. (B) Co-IP of Flag-tagged STAU2 and Myc-tagged UPF1 in HEK293T cells.
1052 Myc-tagged RIP1, a protein not involved in this complex, was not immunoprecipitated
1053 with Flag-tagged STAU2 (right panel), indicating that the interaction seen with UPF1
1054 and STAU2 was not due to promiscuous binding or specific to the Myc and Flag peptide
1055 tags. (C) Flag co-IP as in (B) but incubated with 100 µg/ml RNase A. Note loss of
1056 endogenous RPS6 from complex with RNase A treatment and retention of UPF1. (D)
1057 Co-IP demonstrating that removal of the STAU2 C-terminus along with the TBD (C351)
1058 abrogates binding of UPF1 but has no effect on binding to the ribosome (RPS6). In

1059 contrast, a mutation in dsRBD3 of STAU2 (F207A), but not the full-length or C351
1060 mutation, disrupts ribosomal interactions as indicated by reduced IP of endogenous
1061 RPS6. **(E)** Co-IP of STAU2 proteins harbouring C-terminal deletion mutations. **(F)**
1062 Putative UPF1 binding region in STAU2 based on the co-IP experiments. The homology
1063 of this region compared to STAU1 is low (ClustalW alignment), indicating that the
1064 interaction with UPF1 might be different between these two proteins. **(G)** Immunoblot of
1065 STAU2 and GFP expression in hippocampal neurons expressing scrambled or *Stau2*
1066 RNAi (expressing GFP on a separate cistron; “RNAi virus GFP”) or RNAi plus a rescue
1067 lentivirus expressing the GFP-STAU2 or the C351 mutation constructs that are both
1068 resistant to the rat-specific RNAi. Note the STAU2 antibody used does not detect the
1069 STAU2 C351 species. GAPDH was used a loading control. **(H)** mGluR-mediated
1070 induction of MAP1B protein synthesis requires the UPF1 binding region. MAP1B protein
1071 levels were assessed by immunofluorescence in distal neurites of hippocampal neurons
1072 after 10 minutes following stimulation with 50 μ m DHPG or with vehicle. Neurites from
1073 25-36 neurons and four independent cultures were analyzed. A one-tailed, one-way
1074 ANOVA with Šidák multiple hypothesis correction was used.

1075

1076 **Figure 6. mGluR-LTD in cultured neurons is protein synthesis-dependent yet**
1077 **translation initiation-independent.** **(A)** Representative traces of miniature excitatory
1078 post-synaptic currents (mEPSCs; denoted by dots above traces) over time during whole
1079 cell recording from cultured (18-25 DIV) rat hippocampal neurons. **(B)** Summary bar
1080 graphs for all cells, showing LTD of mEPSC frequency, but not amplitude, 30 minutes
1081 after application of DHPG. LTD was prevented by the translation elongation inhibitor

1082 emetine (40 μ M) but not by the translation initiation inhibitor homoharringtonine (HHT;
1083 20 μ M). Data are accumulated from 4-9 neurons from 4-5 independent experiments.

1084

1085 **Figure 7. mGluR-LTD is impaired by STAU2 and UPF1 knockdown, and its rescue**
1086 **requires UPF1-STAU2 interaction.** (A) Representative traces of mEPSCs during
1087 whole-cell recording from cultured rat hippocampal neurons transduced with indicated
1088 lentiviruses (expressing GFP and/or mCHERRY). (B) Summary bar graphs for all cells,
1089 showing that LTD of mEPSC frequency, but not amplitude, induced by DHPG
1090 (scrambled RNAi-treated cells) is impaired in cells with knockdown of UPF1 or STAU2,
1091 and rescued in cells with RNAi-resistant STAU2 overexpression but not in cells with
1092 overexpression of STAU2 lacking the UPF1 binding region (C351 mutation). Data are
1093 accumulated from 5-9 neurons from 3-6 independent experiments.

1094

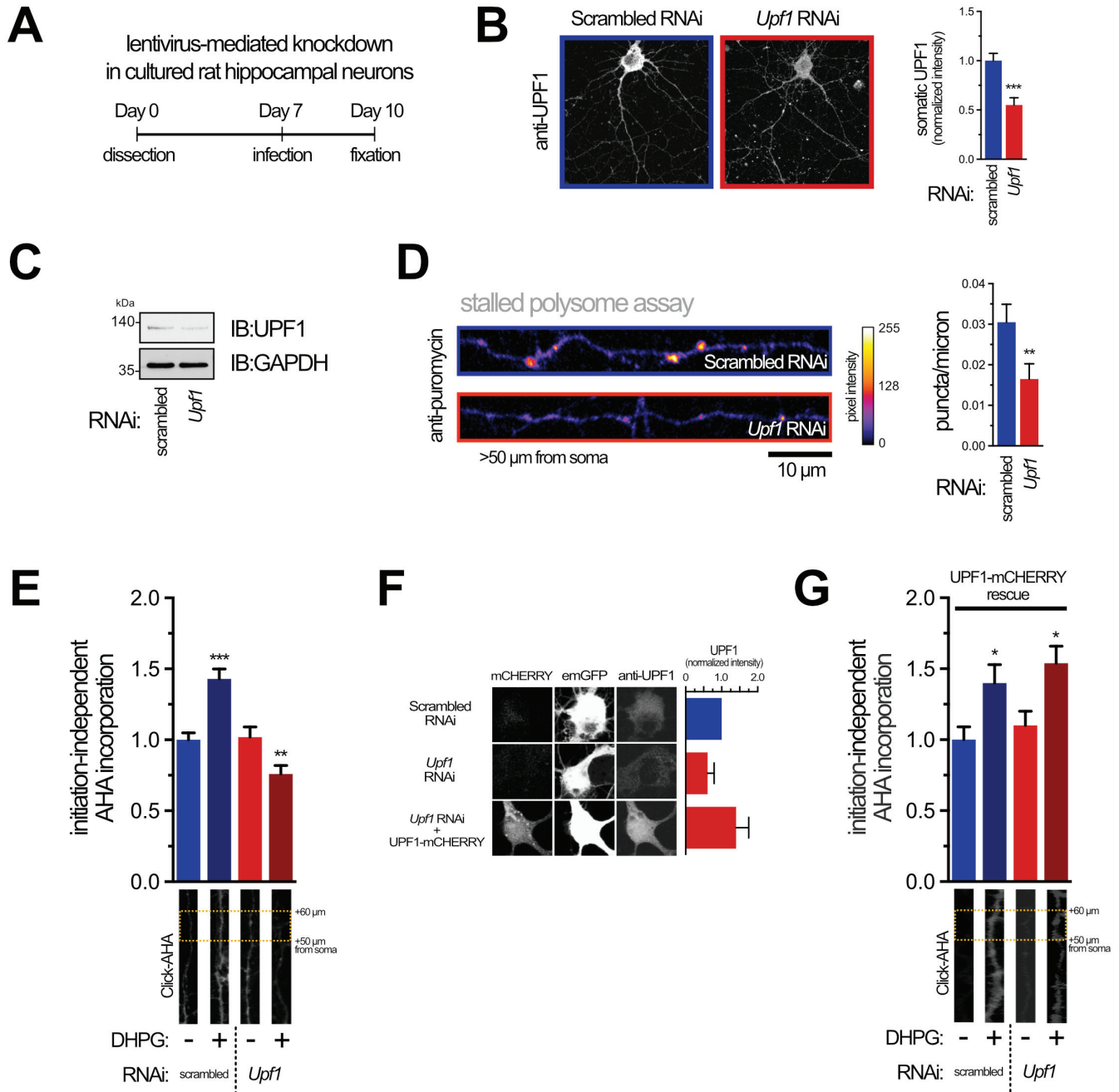
1095 **Figure 8. Model illustrating how UPF1-STAU2 interactions might contribute to**
1096 **local protein synthesis from stalled polyribosomes in synaptic plasticity.** Target
1097 mRNAs such as *Map1b* harbour STAU2-UPF1 complexes in their 3' UTRs that may
1098 prevent proper translation termination (indicated by eRF1 at the stop codon) and/or stall
1099 elongation, thus creating a stalled polysome complex. In the absence of either STAU2
1100 or UPF1, *Map1b* mRNA fails to be transported into neurites. After transport of the
1101 stalled polysome complex to synapses, its reanimation is dependent on UPF1-STAU2
1102 interactions, as mGluR-LTD fails to be expressed in the presence of HHT and a STAU2
1103 mutant protein that still interacts with ribosomes but cannot form a complex with UPF1.

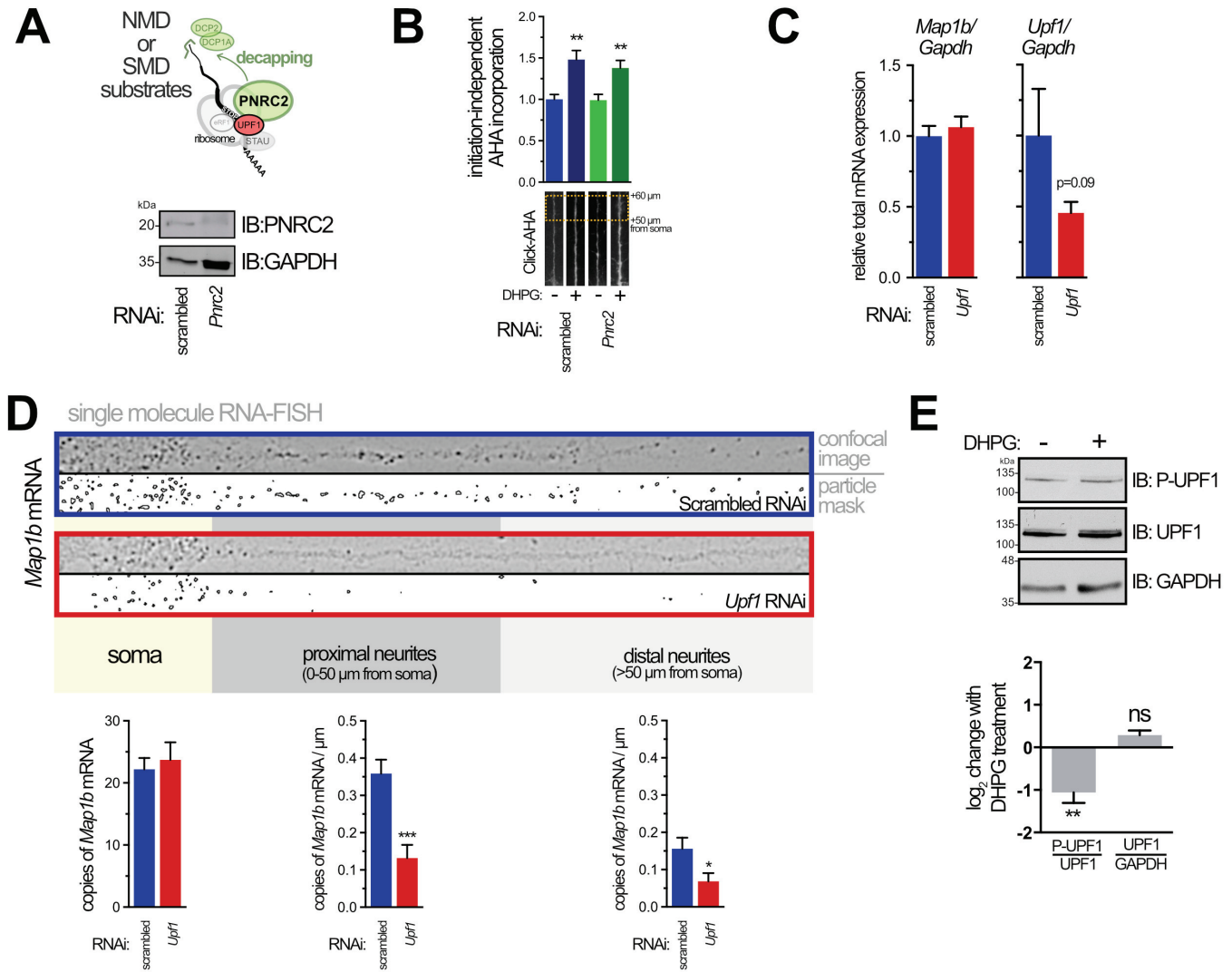
1104 This interaction depends on the tubulin binding domain (TBD) present in STAU2 which
1105 likely mediates interaction with the cysteine-histidine-rich (CH) domain of UPF1.

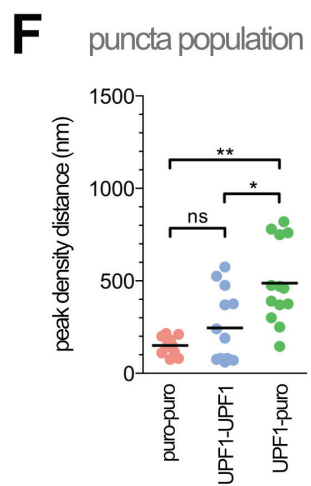
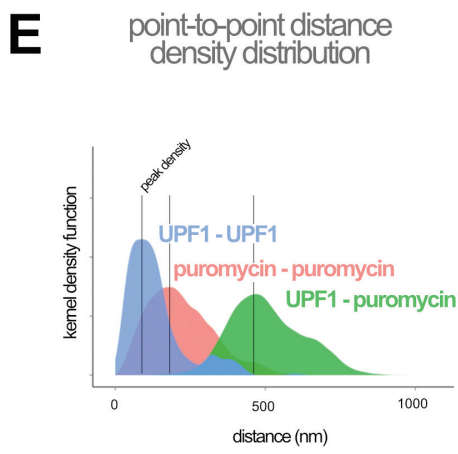
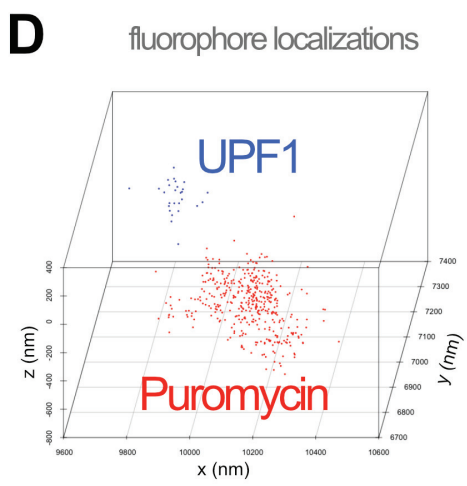
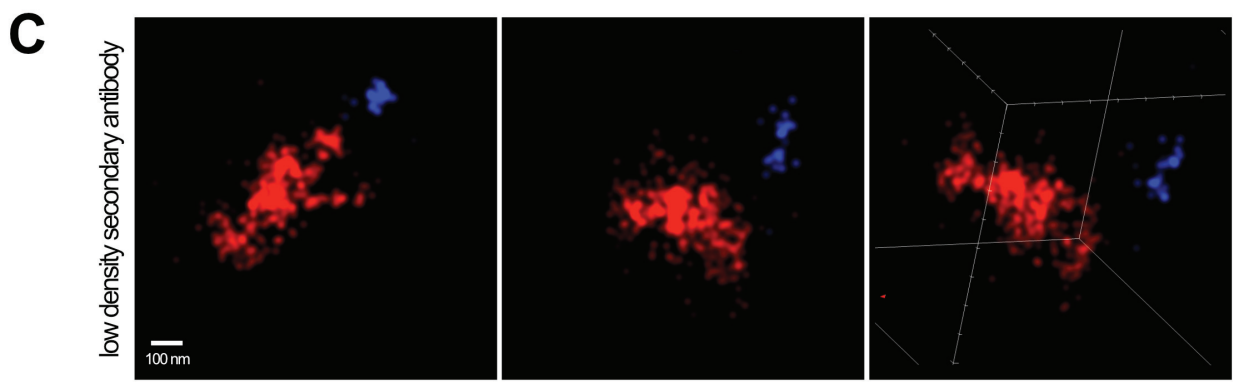
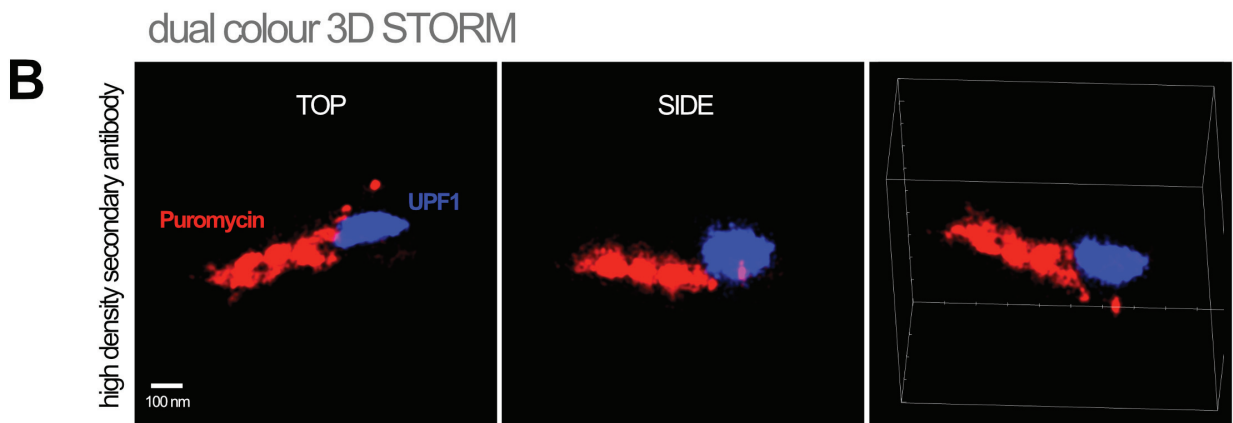
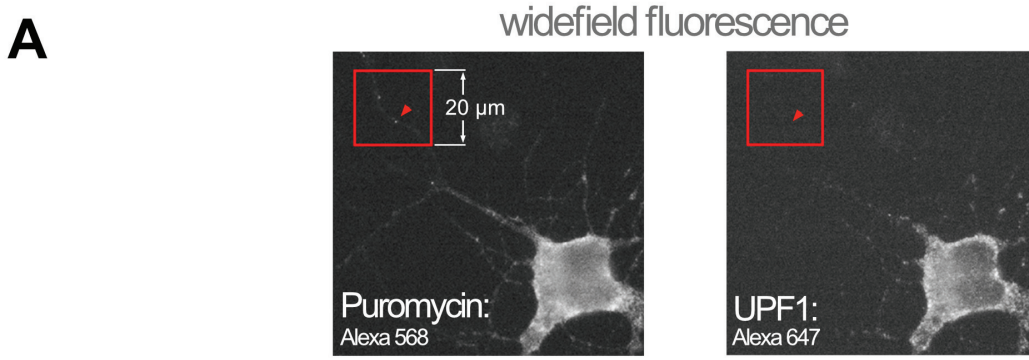
1106

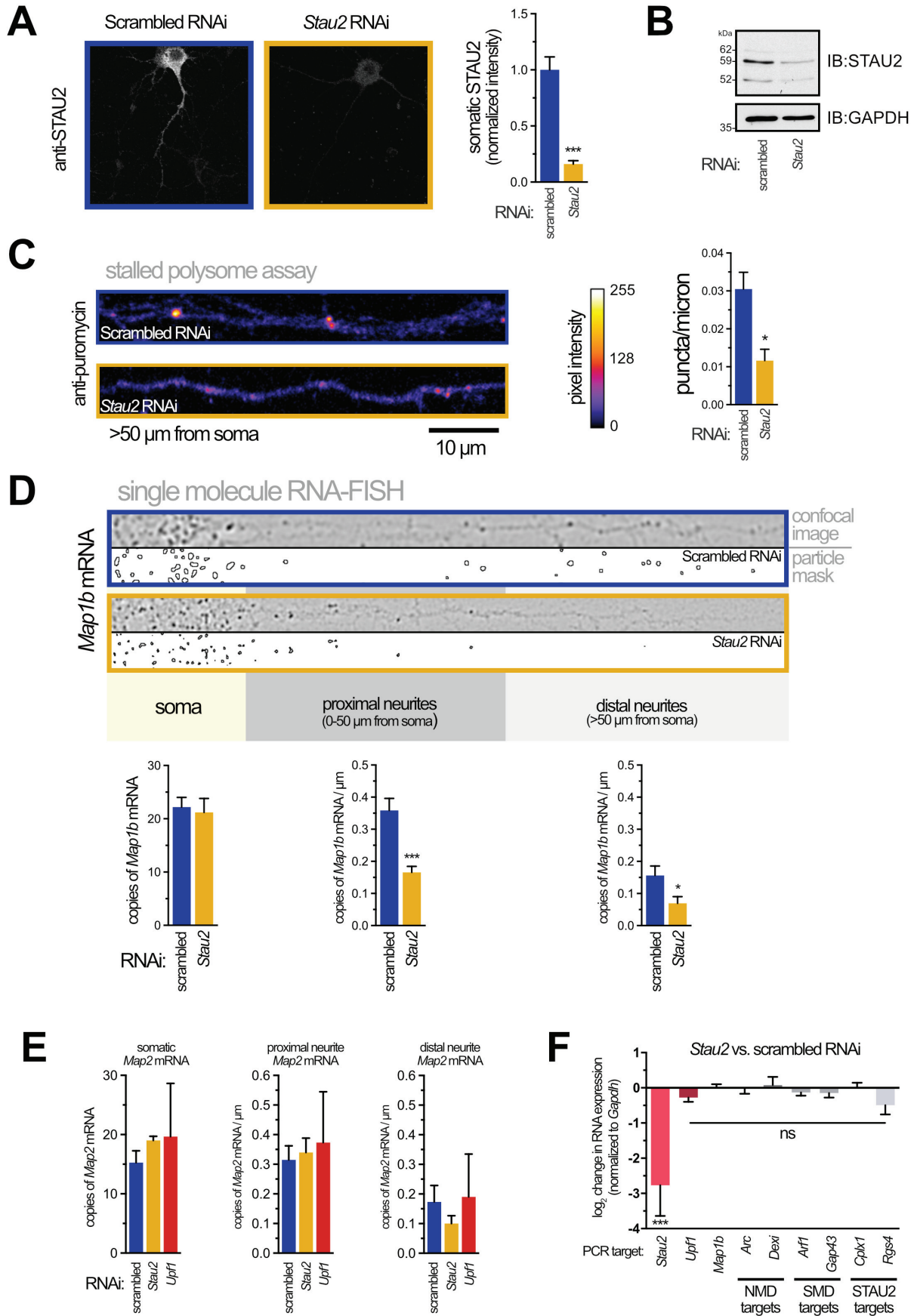
1107
1108

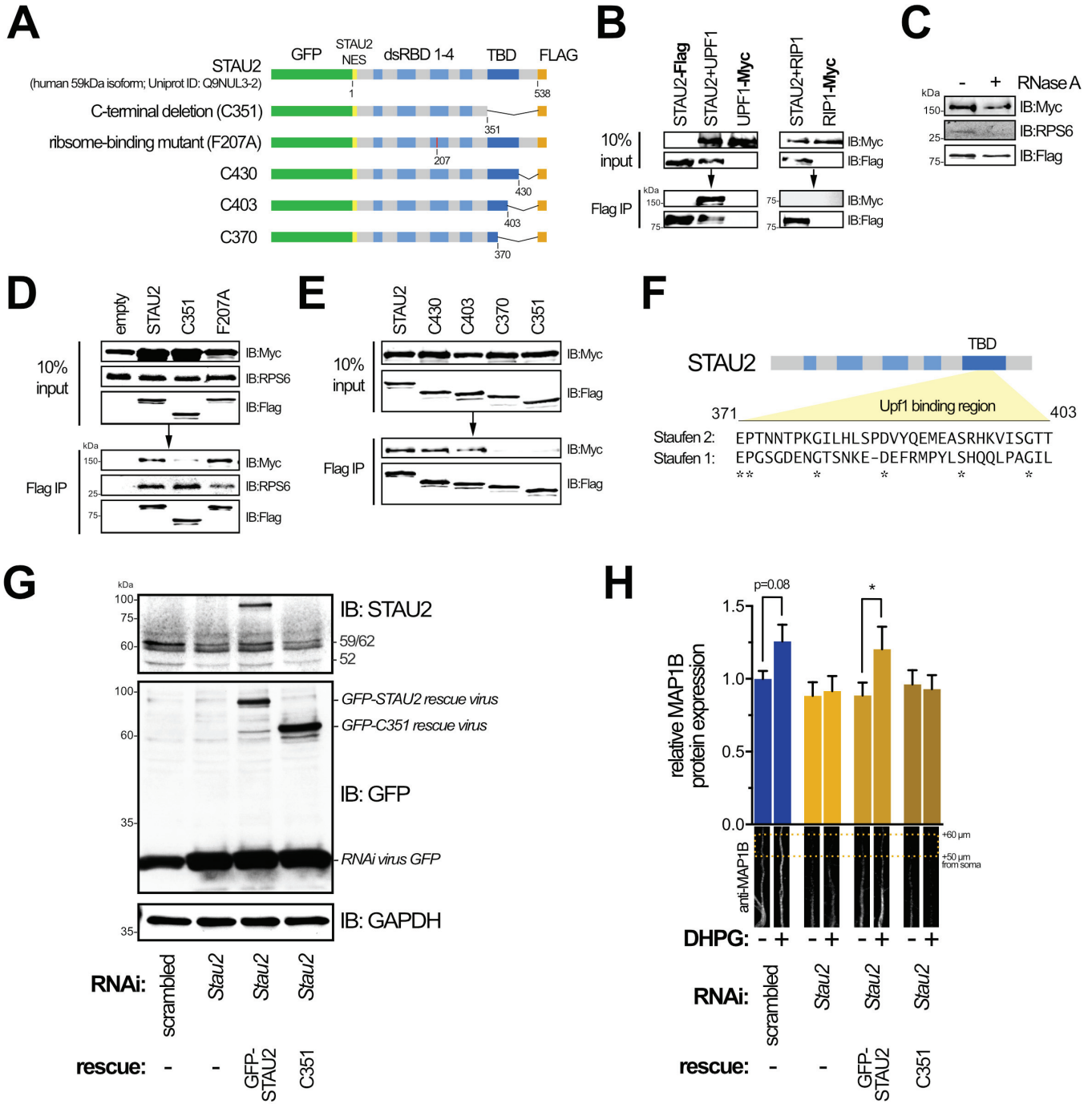
1109
1110





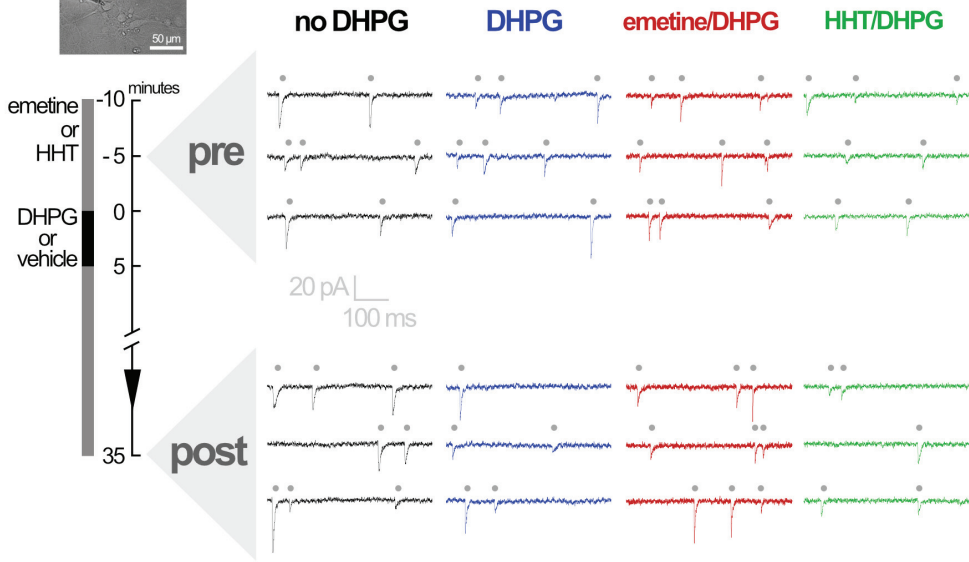
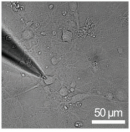




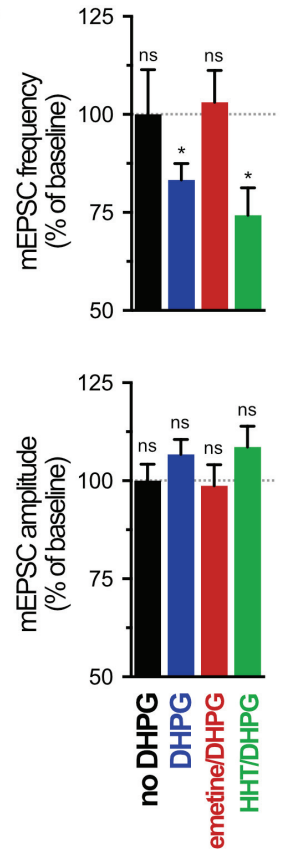


A

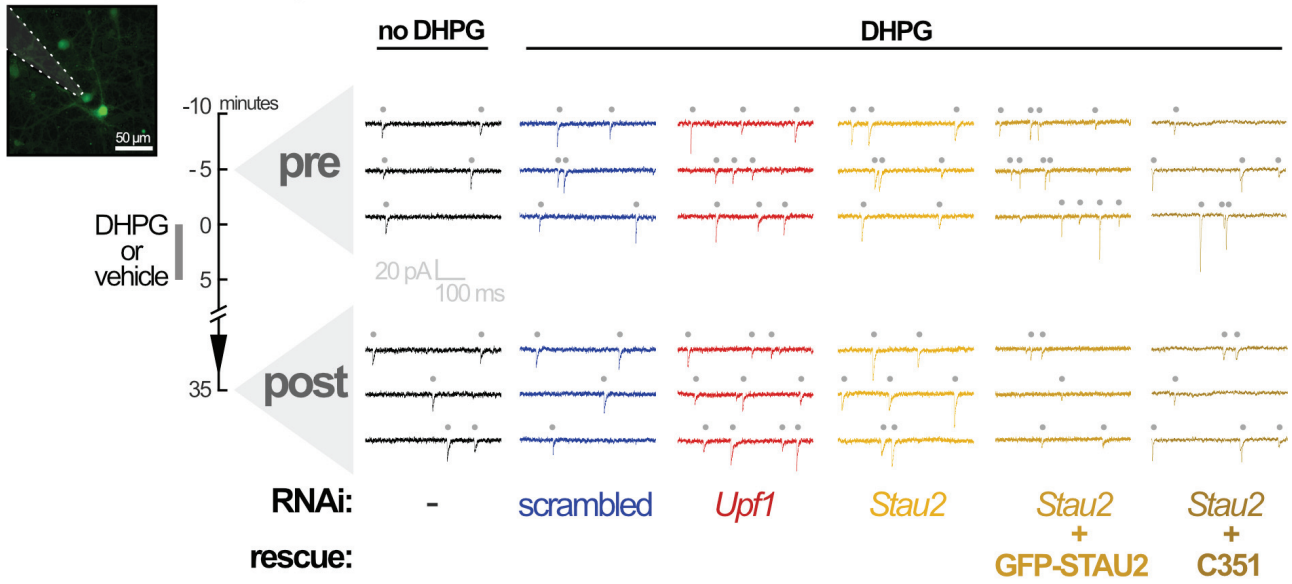
Day 0 - dissection and plating
 Day 18-25 - recording



B



A Day 0 - dissection and plating
 Day 5 - infection with RNAi lentivirus
 Day 18-25 - recording



B

